REMOTE SENSING FOR WETLAND RESTORATION ANALYSIS:

NAPA-SONOMA MARSH AS CASE STUDY

by

Charles Byrne

A professional paper submitted in partial fulfillment
of the requirements for the degree

of

Master of Science

in

Land Resources and Environmental Sciences

MONTANA STATE UNIVERSITY
Bozeman, Montana

May 2019

ACKNOWLEDGEMENTS

I am very fortunate to have benefitted from the wisdom and guidance of Professor William Kleindl, my advisor, for which I am deeply grateful. I am also thankful for the extremely helpful counsel of Professor Scott Powell, a member of my committee.

TABLE OF CONTENTS

LIST OF FIGURES

ABSTRACT

Human-caused ecosystem change and habitat loss is a major worldwide concern. Wetland loss has been remarkable worldwide and in the US. In the San Francisco Bay system, the largest estuary on the eastern rim of the Pacific Ocean and a biodiversity hotspot, more than 90 percent of the wetlands have been lost to urban development, salt production and agriculture, a loss that primarily occurred in the century following 1850.

Restoration is our primary mechanism for confronting this challenge. While wetland restoration design has advanced dramatically since the early designs of the 1980s, restoration analysis and evaluation remain challenges that until now have wholly or primarily required on-site sampling. This is a major challenge for larger restoration projects, such as the Napa-Sonoma Salt Marsh restoration in California.

Previous studies have indicated that the Normalized Difference Vegetation Index (NDVI) has been used in some restoration analyses with apparent success, but data is limited. To better understand its potential, this study examines issues in restoration analysis in the context of wetland restorations. By comparing pre- and post-restoration remote sensing data, I found that two sites in the Napa-Sonoma Marsh restoration demonstrated mixed NDVI results and that changes depended on subarea and whether median or maximum NDVI was analyzed. The mixed results are explained by several factors: the inherent limitations of NDVI; the large restoration size; the fact that wetlands, less vegetated, present special challenges for analysis; and the fact that it is early in the post-restoration period.

The case study supports the use of remote sensing and GIS for restoration analysis and evaluation, but also emphasizes their current limitations. Many of these limitations, which hinge on the complexity of the potential data involved, are likely to be addressed in the next generation as the relevant technology continues to develop.

INTRODUCTION

1. Study Context

The need for ecological restoration will likely grow considerably in coming years as awareness increases of the need for maintaining natural areas in the face of increasing human population and impact. Worldwide wetland loss as of 2009 was estimated at 33% (Hu et al., 2017) and in the US, it has been estimated that nearly half of the wetlands in the continental states were eliminated by the 1970s (Batzer & Sharitz, 2014). For example, the San Francisco Bay system is the largest estuary on the Eastern Rim of the Pacific Ocean and a biodiversity hotspot, yet more than 90 percent of its wetlands have been lost to urban development, salt production and agriculture. These losses occurred in a relatively short period, mainly in the century following 1850 (Barnum, 1996).

Restoration is our primary mechanism for confronting this challenge. While restoration design has advanced dramatically since the artifices of the early 1980s, restoration analysis and evaluation have not kept pace with advances in remote sensing technology and have required on-site sampling. Analysis of restoration progress and evaluation of its success are vitally important in the process of restoration. Yet field observations are time-consuming and costly, particularly for large restorations; further, they may be prone to certain statistical biases avoidable with remote sensing analysis.

Increasing remote sensing capabilities have revealed the enormous potential for large-scale restoration analysis; satellite technology has improved substantially since the 1970s and promises increasing spatial and temporal resolution. Geographic Information System (GIS)

software provides greater flexibility for automatic analysis of the resultant images. However, remote sensing must be verified as a suitable tool for restoration analysis, and evidence is still scant.

The Normalized Difference Vegetation Index (NDVI) and other modes of analysis collectively offer a plausible baseline for large-scale restoration analysis, but whether remote sensing can soon supplant field observations requires examination. Previous studies have suggested that NDVI has been used in some restoration analyses with apparent success, though data are limited. To better understand the potential, this study examines questions of restoration analysis in the context of wetland restorations. Any restoration analysis must address complex variables, but change analysis with NDVI offers an important first step in the evaluation of a wetland restoration.

2. Napa-Sonoma Marsh

Napa-Sonoma Marsh Historical Geological Context

The Napa-Sonoma Marsh is a tidal salt marsh that sits on San Pablo Bay in California at about 38 degrees latitude, between the Sonoma Creek and the Napa River. It is part of the larger – and, at about 10,000 years old, relatively young – San Francisco Bay system (also known as the 'San Francisco Estuary'). The San Francisco Bay is a 'drowned river valley' (Josselyn, 1983) lying in a tectonic valley between the San Andreas and Hayward Faults. Its waters have been ephemeral since its valley was first flooded one million years ago (Sloan, 2006). About 20,000 years ago (during the last ice age), the seas were lower and the California shoreline was situated about 50 km west of the Golden Gate. Currently, San Francisco Bay carries the freshwater runoff

for 40 percent of California, despite the fact that municipal and agricultural diversion has reduced the inflow to 60 percent of the pre-1850 flow (Sloan, 2006).

North of the Marsh lie diverse rock formations from the past 200 million years. The oldest rocks formed via plate collision, subduction, and accretion during the Mesozoic and early Tertiary Eras when Western California was subsumed under the Pacific Ocean, and the youngest rocks are from volcanic activity about 10,000 years ago. Marshes like the Napa-Sonoma comprise unconsolidated sediments (Sloan, 2006).

Napa-Sonoma Marsh Land Use History

The general outline of the Marsh is recognizable in old charts and maps; see, for example, Figs. 19–21 in Appendix A. However, the hydrology is substantially different than it was 150

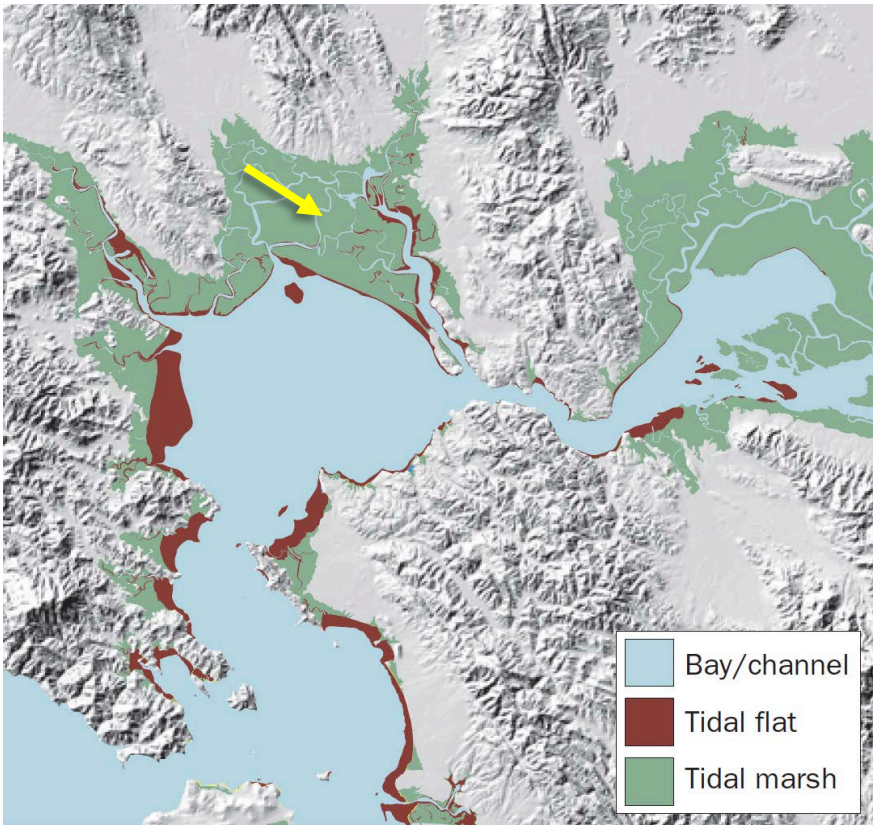

Figure 1: Historic wetlands of San Francisco Bay (Sloan, 2006, Figure 33a).

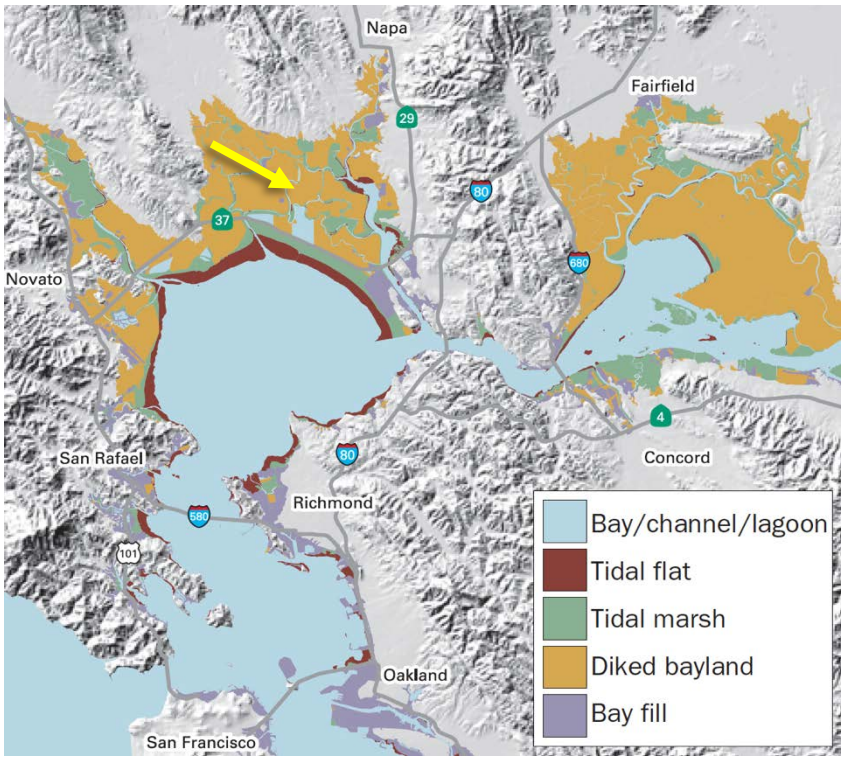

Figure 2: 2006 status of wetlands of the San Francisco Bay (Sloan, 2006, Figure 33b).

years ago, before diking and salt production began in earnest. Figs. 1 and 2 summarize the changes that the Marsh (yellow arrow) has undergone and that the restoration attempts to reverse. The 1902 map shown in Appendix A (Fig. 21) also shows the encroachment of European-American development – there is an urban presence (Vallejo), other structures, and even a railroad that traverses the Marsh.

The shoreline of the San Francisco Bay is now largely artificial fill that dates to the mid-19th-century forward; the present surface area of the bay is about 40 percent less than its historic surface area. Ninety-five percent of the once-extensive mudflats and marshes on the Bay have been destroyed by diking and filling for agriculture, industry, and urban development, and raw

sewage was freely discharged into its waters for much of the 19th and 20th centuries (Sloan, 2006). By the 1950s, it was projected by some urban planners and environmentalists that the Bay would eventually be entirely filled in (*Saving the Bay*, 2009). The 1960s saw a nascent environmental movement that spurred changes to halt some of these effects.

Prior to first European contact, Native Americans collected salt in the wetlands along the Bay with little resultant impact. After the gold rush of 1849, industrial salt production ramped up. Salt ponds were likely created not much later than 1860 at Napa-Sonoma. By early in the 20th century, the Marsh had been transformed, altered by diking for industrial salt production and regular human presence. Fig. 3 indicates the stark developments in wetland status changes in San Francisco Bay since 1800. The changes also present opportunities for restoration, however, and another large restoration has been undertaken east of the Napa-Sonoma Marsh at Suisun Marsh.

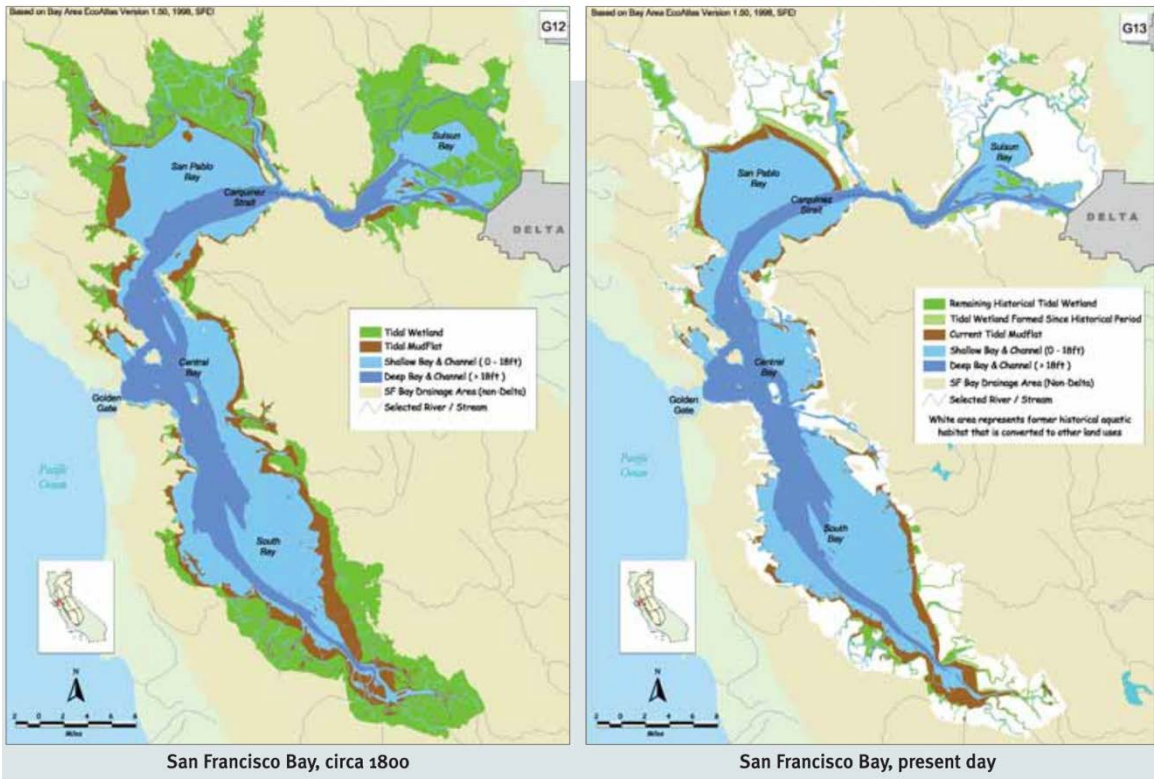

Figure 3: San Francisco Bay wetland loss – and restoration opportunity – 1800 to present day (Pescovitz, D., 2008). On the top left is Napa-Sonoma Marsh. & on the top right is Suisun Marsh, also undergoing restoration.

As a case study, I analyzed two parts of a large Northern California estuarine restoration. The Napa-Sonoma Marsh Restoration Project is a 67 km^2 (Landers, 2003) tidal marsh, situated north along San Pablo Bay in the northern part of San Francisco Bay, between Sonoma Creek on the west and the Napa River on the east, and abutting the San Pablo Bay National Wildlife Refuge. Fig. 4 shows the site as of 2013, or in the latter stage of restoration. I examined two portions of the larger project – the former salt ponds, which comprise 41.3 km^2, and the former salt plant, which comprises 5.2 km^2. Fig. 5 conveys these two sites in the context of the numbered pre-restoration salt ponds and salt plant (what became the North, Central, and South Units); the Marsh site is labeled therein as 'Wildlife Area', as 13,000 acres are so designated (Huffman, 1999). In the 1990s, the state acquired the land with the intention of restoring it to

Figure 4: Napa-Sonoma Marsh restoration as of 2013
(image by Russ Lowgren, Ducks Unlimited, in Okamoto, 2013).

wetlands. Initial levee breaches occurred in the 1990s, Phases I and II were completed by 2006, and Phase III was completed in the last 1-2 years (Erickson, 2018).

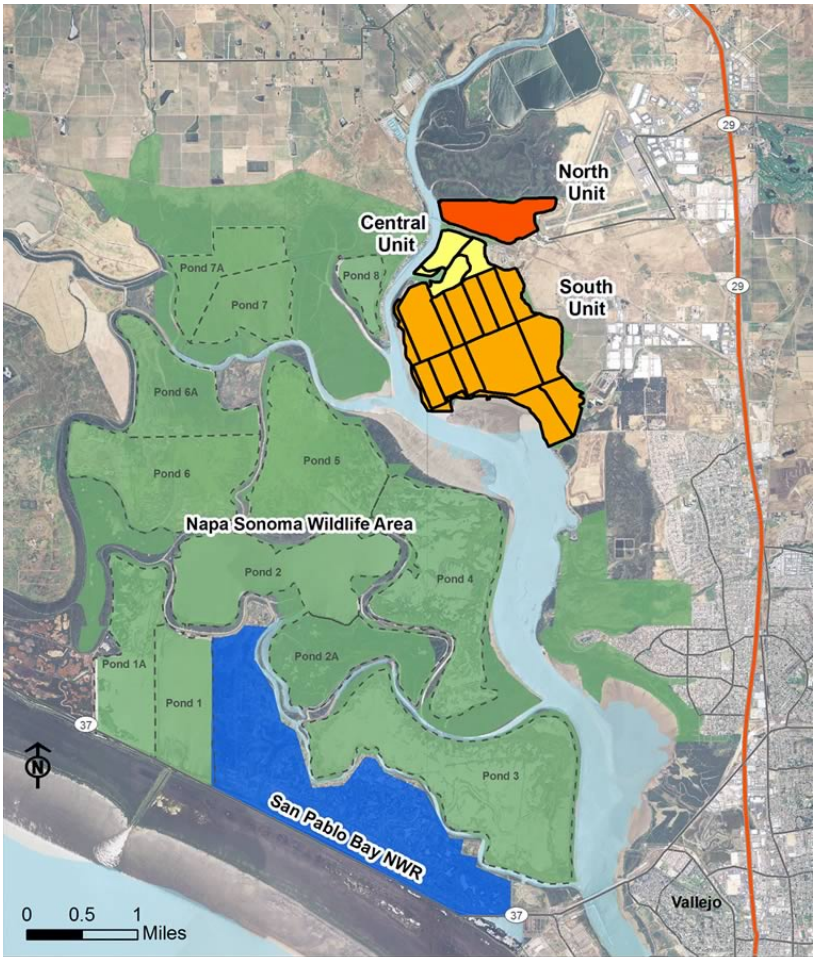

Figure 5: Lower Napa River wetland restoration locations (Okamoto, 2013).

The Marsh is an important site for birds, including federally-listed species, and other wildlife; further, it may provide a natural buffer for impending sea level rise. However, it is also vulnerable to that sea level rise, as well as challenges that accompany any restoration, so ongoing monitoring will assess whether the construction measures have created an adequate system for something akin to self-maintenance and one that is good habitat for wildlife. The Marsh's location near expanding high- and medium-density urban areas (Vallejo, CA, abuts the Napa River to the east, for example) is also a source for significant concern.

Benchmark restoration dates utilized in this study are 1994, when purchase of the Salt Ponds was made by the State of California; 2006, when the major phases of construction were completed; and present day (2018, the most recent year available), with the restoration essentially complete (Erickson, 2018).

3. Literature Review

As Batzer & Sharitz (2014) note, 'forty years ago, the practice of wetland restoration was so rudimentary that, regardless of the kind of wetland ecosystem and services that were damaged or destroyed, a common remedy was to replace it with a pond' (Batzer & Sharitz, 2014). However, wetland restoration design and practice has improved enormously in the intervening period. The Napa-Sonoma Marsh is a prime example, and the amount of planning and activity that have gone into its restoration design and implementation – 20–30 years, depending on what one regards as the starting point – reflect the resources that a large restoration during this period has entailed. As part of the practice of restoration, analysis of site's status and evaluation of its progress have also matured. However, these practices, until recently, were completed strictly via on-site sampling, and often still are.

Klemas (2013), in an overview of the use of remote sensing to monitor wetland restoration, found that it can be accurate and cost-effective. His 2011 analysis of case studies also found that remote sensing data from satellites and aircraft is an effective tool when combined with local observations (Klemas, 2011). In an early study, Phinn et al. (1996) found that remote sensing (high-spatial-resolution digital video, with a 0.8-m-pixel resolution) offered an approach complementary to field sampling in evaluating the potential of restored wetland in San Diego

County to provide suitable vegetation and spatial expanse for the Light-footed Clapper Rail, given that it was accurate, noninvasive, and cost-effective (Phinn et al., 1996).

Shuman & Ambrose (2003) compared three vegetation sampling techniques, one of them remote, for a restored Pacific Coast wetland dominated by *Salicornia virginica* (perennial pickleweed), and found that aerial photography was both more efficient for assessing large areas and was accurate in sampling vegetative cover, but was unable to identify individual species (Shuman & Ambrose, 2003). Selvam et al. (2003) analyzed mangrove wetland restorations in Pichavaram, India using TM (1986, before restoration) and LISS III (2002, after restoration) data (via the Landsat 5 and Resourcesat-1 satellites, respectively). They found that mangrove forest area had increased by about 90% and that remote sensing was an effective solution to monitor restoration where local monitoring is difficult (Selvam at al., 2003).

Abtew & Melesse (2013) studied wetland restoration sites in Northwestern Minnesota and Southern Florida and found that remote-sensing-based evapotranspiration analysis was effective for monitoring wetland hydrology (Abtew & Melesse, 2013). Riegel et al. (2013) compared types of remote sensing in a restoration context, LiDAR and high-resolution optical imagery for modeling above-ground carbon biomass at a recently-restored forested wetland in Eastern North Carolina. They found that the optical imagery explained more observed variation than the LiDAR and was better able to predict biomass extremes. Combining both models offered only marginal improvement, so optical imagery was determined to be preferable for a recent forest restoration (Riegel et al., 2013).

To quantify vegetation change within the Nisqually River watershed in Washington, Ballanti et al. (2017) produced time-series classifications of habitat, photosynthetic pathway functional types and species for the years 1957, 1980, and 2015, using remote sensing data. They found that restoration produced a 44% net increase in emergent marsh wetland within the Delta

between 1957 and 2015, and that the coincidence of the trajectory of this recovery with previous studies pointed to the accuracy of remote sensing for coastal wetland monitoring (Ballanti et al. 2017).

By evaluating modeling by means of combined data from local digital cameras and Landsat for two restored freshwater marshes in the Sacramento–San Joaquin River Delta in California, Knox et al. (2017) found that remote sensing is an effective tool for modeling carbon variation. Their model was able to explain up to 91% of the variation in daily gross primary productivity (GPP) in the marshes and to predict annual GPP budgets within 0% to 20% of observed budgets. However, they also found that model performance decreased with increasing site complexity, and that Landsat data in particular performed better in homogenous than in heterogenous environments (Knox et al., 2017).

Two relevant studies in the literature studied locations near the Napa-Sonoma Marsh. Newcomer et al. (2014) modeled sediment deposition within recent pond restorations in the industrial salt flats of San Francisco Bay using Landsat 5 and ASTER data and via three techniques: linear regression, multivariate regression, and artificial neural network (ANN) regression. They found multivariate and ANN regressions with ASTER data to most accurately correlate with reference data (Newcomer et al., 2014). Tuxen et al. (2008) used a semiautomated technique with color infrared aerial photography and NDVI to document vegetation in Petaluma Marsh, a restored salt marsh in San Pablo Bay. They found that high-resolution remote-sensing data can be very effective in monitoring change in a rapidly-vegetating wetland, but that long time frames with yearly image acquisition are required (Tuxen et al., 2008).

Finally, Lumbierres et al. (2017) argued that 'proxies of aboveground biomass' like NDVI and the Enhanced Vegetation Index (EVI) can produce misleading results, such as when they 'saturate asymptotically at high biomass values' (Lumbierres et al., 2017).

4. Research Question

In light of these challenges, my research question was whether NDVI data obtained via remote sensing are sufficient for restoration success analysis and evaluation. The methods below were designed, in part, to examine NDVI data at different temporal and spatial resolutions.

METHODS

1. Case Study Area

The study area comprised two sites (Fig. 6): the 'Marsh' site (41.3 km^2) and the 'Salt Plant' site (5.2 km^2). Source maps (Carroll, 2007; San Francisco Bay Joint Venture, 2018), were used to delineate the two sites by the construction of two polygon 'geometries' in Google Earth Engine. These geometries were imported into numerous scripts for various analyses.

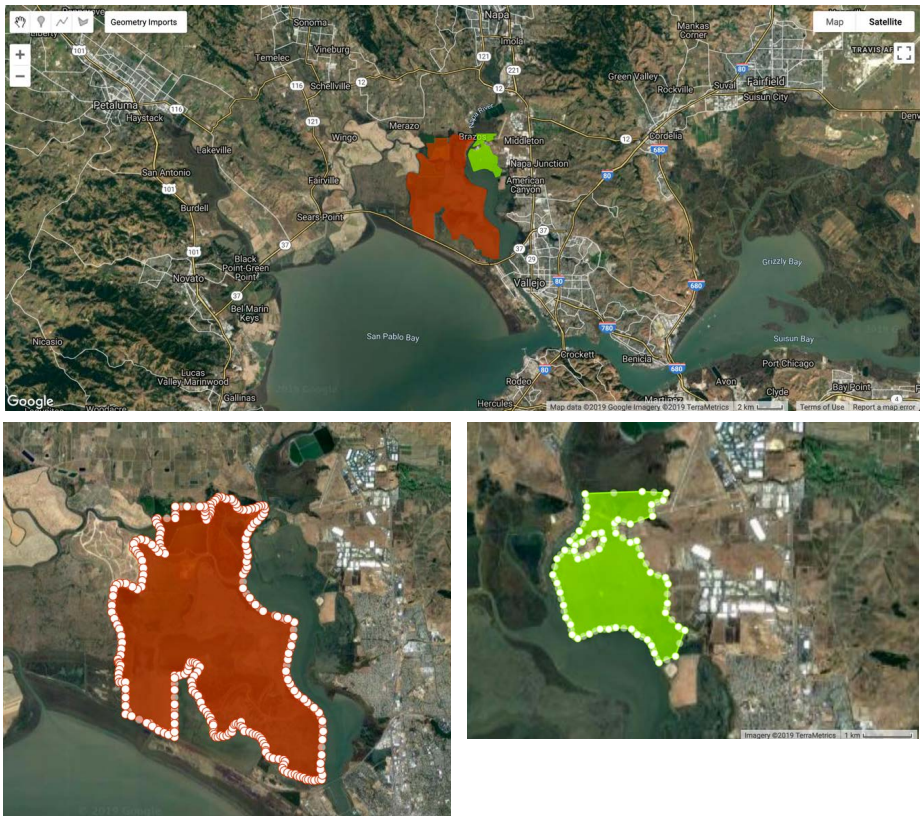

Figure 6: Top: Two site polygons constructed in Google Earth Engine.
Bottom: magnified, with markers – Marsh (left), Salt Plant (right).

2. GIS: Google Earth Engine

I analyzed data using the web-based geographic information system Google Earth Engine (GEE) – a 'cloud-based platform for planetary-scale environmental data analysis', combing datasets, parallel processing cloud computing, application programming interfaces (APIs), and a code editor (Google, n.d.). GEE allows for greater resources, programming flexibility, and computing power to perform analyses in real time than other publicly available platforms.

3. Normalized Difference Vegetation Index and Other Data

As noted in the literature review above, there is a general agreement that the Normalized Difference Vegetation Index (NDVI) represents vegetative vigor and has great potential for detailed, long-term tracking of vegetation in restorations.

NDVI's formula of

$$(NIR - R)/(NIR + R)$$

was calculated using the NIR (near infrared) and R (red) bands of the three relevant Landsat satellites (see below). NDVI values range from –1 to 1. Positive values of 0.1 indicate rock, sand and snow; 0.3, sparse vegetation; 0.6, temperate forests; and 1.0, the highest possible density of vegetation (e.g., rainforest) ("Measuring Vegetation (NDVI & EVI)," 2000).

Because NDVI is intended to be based on reflection from surfaces themselves, it is critical to exclude images that contain clouds or other obstructions, or compensate for them. In this study, data trends were analyzed from SR ('surface reflectance') image data, so that data underwent post-collection processing for atmospheric correction, including cloud, shadow, water and snow masks. For the sake of comparison, and because some periods featured

more complete data for it, some qualitative data here used TOA ('top of atmosphere') data, which compensates for satellite position but not for atmosphere; however, the data, based on annual medians and maxima, avoided cloud problems even with TOA data. SR and TOA processing were available for images from each of the three satellites utilized in this study. Further, all images were Tier 1, which indicates high-quality data that is also inter-calibrated across all Landsat sensors.

NDVI was chosen as the vegetation index (VI) in this study because it is widely used, previous studies have advocated for its use, and no other VI was clearly preferable. Older studies from the 1970s and 1980s have suggested that 'in practice, there are few differences between the many VIs that have been proposed' (Campbell & Wynne, 2011). The more recent Enhanced Vegetation Index (EVI) is seen as the principal alternative to NDVI; it is similar in principle to NDVI, but its more complex formula is meant to correct for atmospheric distortion and for ground cover below the vegetation ("Measuring Vegetation (NDVI & EVI)," 2000). However, particularly for the latter element, EVI is generally regarded as being more favorable in high-vegetation contexts, such as rainforest, contrary to the sites in question here. In addition, atmospheric effects were addressed in other ways, such as by using SR, in this study. Hence, the use of EVI was unwarranted.

I also analyzed precipitation via the Climate Hazards Group InfraRed Precipitation with Station (CHIRPS) daily dataset for the period (1984–2018) in this study. A sample of data was cross-checked against NOAA data for nearby Vallejo.

NDVI Data Acquired with GEE

For the central data analysis for the case study, I obtained data from the Landsat 5, Landsat 7, and Landsat 8 missions (all Tier 1, with time series all SR):

- Landsat 5 (TM): data from period 1984–2011.
- Landsat 7: 2011–13.
- Landsat 8: 2013–18.

I used Landsat 7 data only to fill in the gap between Landsats 5 and 8. Landsat 7 data is regarded as undesirable due to its infamous hardware failure in 2003. However, while data loss has occurred since then, the loss is about 25% and occurs in a predictable pattern; hence, it has been possible to combine data from multiple acquisitions to fill in the gaps (NASA, 2019). I deemed this enough justification to use where data would have otherwise been absent between the Landsat 5 and 8 missions. For Landsat 5 (Thematic Mapper (TM) sensor) and Landsat 7, bands 4 (NIR) and 3 (R) were utilized for NDVI; for Landsat 8, the corresponding bands are 5 and 4.

GEE permits numerous command possibilities for NDVI calculation. Scripts were developed from numerous sources, but primarily Google Earth Engine documentation (Google, n.d.), with modifications from sites such as Stack Overflow ("StackOverflow: Google Earth Engine," n.d.). Non-Google citations, where available, are indicated in script comments.

Images were produced in GEE for annual median NDVI values for 1984 (first year of period, representing the active salt production facility); 1994 (year land was obtained and restoration of Marsh site commenced); 2006 (year that major earth-moving operations at Marsh site were completed); and 2018 (most recent complete year of data).

NDVI difference images, which subtract earlier NDVI values from later ones per pixel to illustrate NDVI changes over time, were completed via median annual NDVI and via maximum annual NDVI for the following year pairs: 1984 and 2018; 1994 and 2006; 2006 and 2008; and 2013 and 2018 (the last representing the most recent 5-year period). Rainfall data obtained via CHIRPS for 1984–2018 was also downloaded as a .csv file.

4. Data Manipulation and Statistical Analyses

Three time-series periods were analyzed:

- 1984–2018 (pre- and post-restoration).
- 1994–2018 (restoration commencement to most recent whole year).
- 2006–18 (post-major Marsh restoration to most recent whole year).

The following analyses were performed for those periods:

- Annual median and maximum NDVI values, per site and combined sites, were calculated using standard formulae in Excel.
- Line graphs of annual median and maximum values and their trendlines and R^2 values.
- Regression analysis (*p*-value; equivalent to *F*-test significance value for one variable) were calculated from the regressions that the line graphs represented.

RESULTS

1. Quantitative Data Results

Quantitative data downloaded from GEE and analyzed in Excel showed trends for median annual NDVI and maximum annual NDVI. Most, but not all, trends were statistically significant. Figs. 7 and 8 show median NDVI time series graphs, first for the entire study period and then for either the 'latter-' or 'post-restoration' period.[1] Data represents the combined sites (Marsh and Salt Plant) in each case.

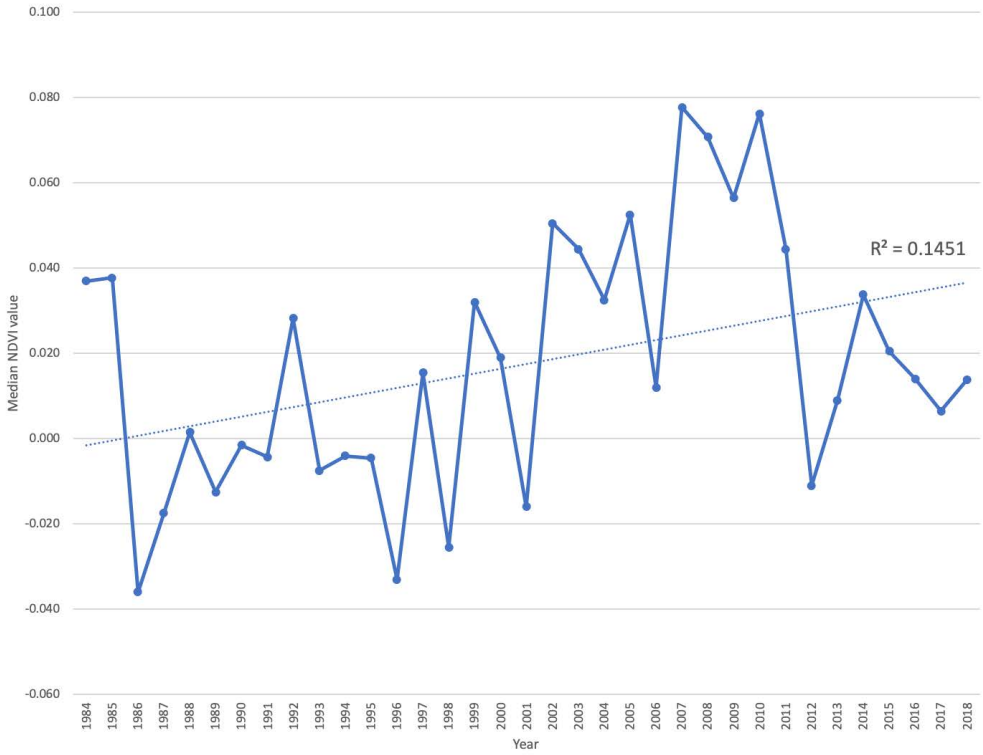

Figure 7: Combined sites, annual median NDVI, 1984–2018 (Landsats 5, 7, & 8 SR).

[1] To reiterate, major earth-moving operations were completed for the Marsh by 2006; however, restoration was not fully completed until 2017 (and even then, the restoration is monitored and it is possible that additional interventions could occur). The Salt Plant site's restoration was 2003–10, with major operations occurring early in that period.

There is a weak positive trend for 1984–2018 (R^2 = .16); this is statistically significant if we take p < .05 (equivalent F-test significance for the case of one variable) as a limit; p = 0.02. The negative trend for the period 2006–18 alone (R^2 = .34) is also significant (p = 0.04). Median trends are

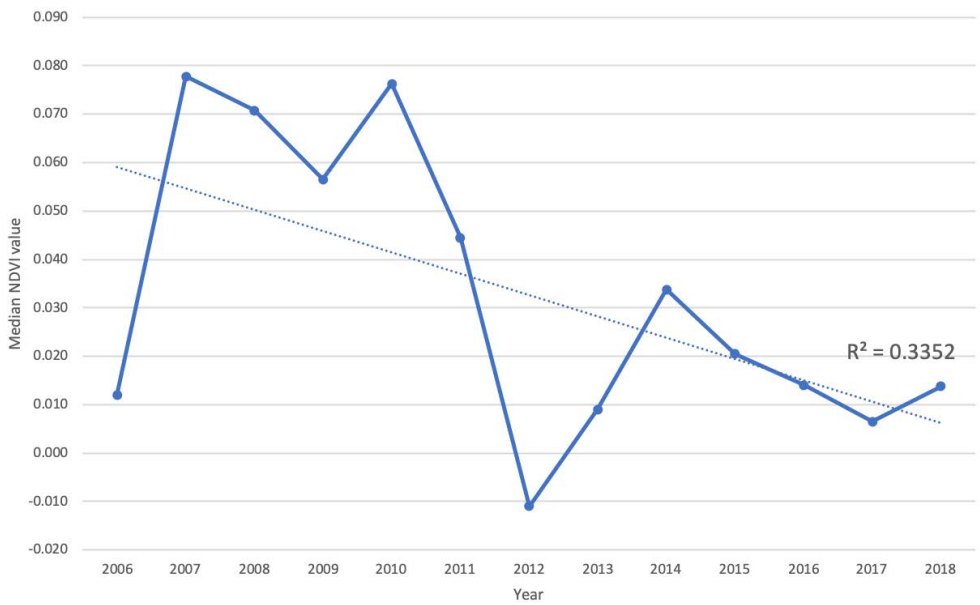

Figure 8: Combined sites, annual median NDVI, 2006–18 (Landsats 5, 7, & 8 SR).

dissimilar for the larger Marsh and smaller Salt Plant sites; in all cases, Salt Plant has more positive NDVI trends. This is likely explained by the incongruous restoration activities in the two sites and the fact that the Marsh site is larger. Further, NDVI median values in nearly all cases were low, though they were higher in the Marsh (reaching about .15 at times) than in the Salt Plant (where NDVI was frequently below zero and only once breached .05).

The trend for the combined-site maximum NDVI – i.e., the addition of annual maximum NDVI values for each site – is again much more strongly positive for the Salt Plant site than the Marsh site (Figs. 9 and 10). The maximum NDVI trend for 1984–2018 is strong at R^2 = .51; this is significant (p = 1.4E-06). The still-positive, though weaker, trend for 2006–18 alone (R^2 = .25) is not significant (p = 0.08).

CHIRPS daily precipitation data (Fig. 11; the trendline is near the baseline and hence difficult to see in the image) shows a flat trend (R^2 = 4E-08), despite drought years in the region for 2006–10 & 2012–18; the same is true for the years 2004–19 alone. This implies that rainfall cannot be taken to be an explanatory variable.

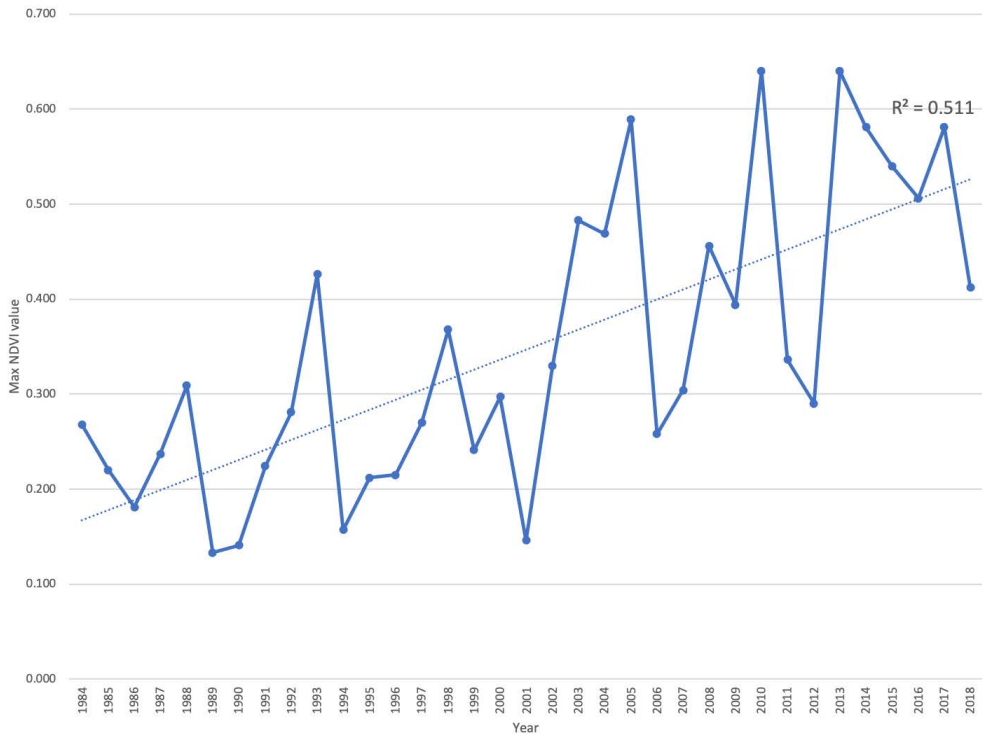

Figure 9: Combined sites, annual maximum NDVI, 1984–2018 (Landsats 5, 7, & 8 SR).

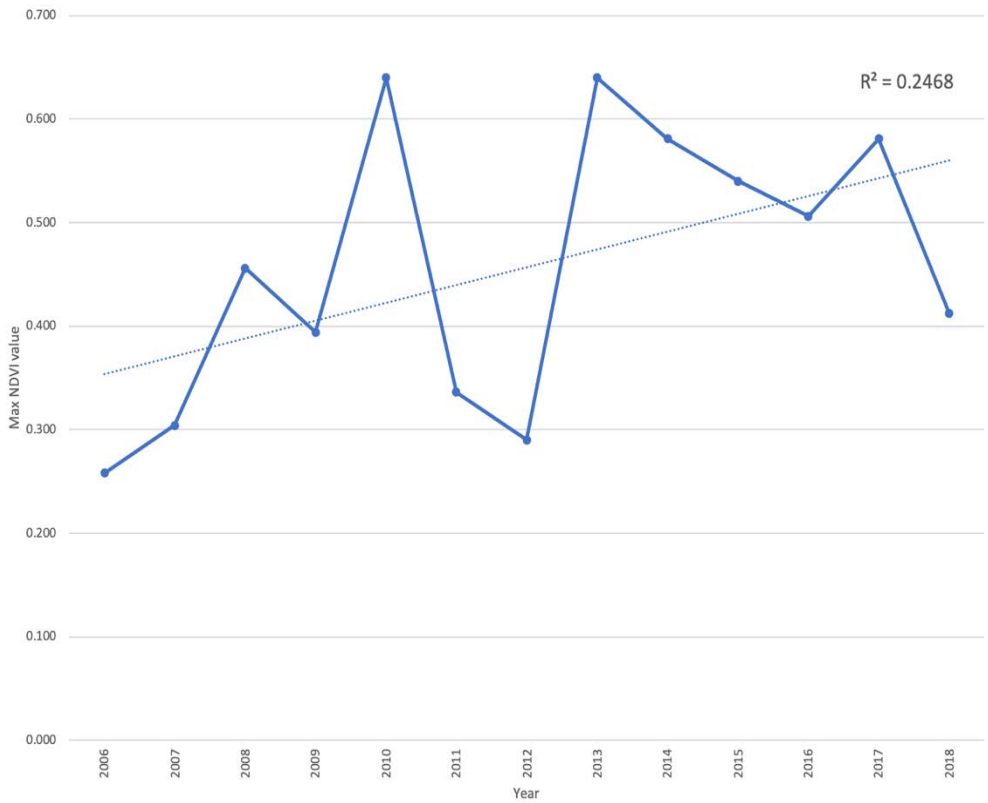

Figure 10: Combined sites, annual maximum NDVI, 2006–18 (Landsats 5, 7, & 8 SR).

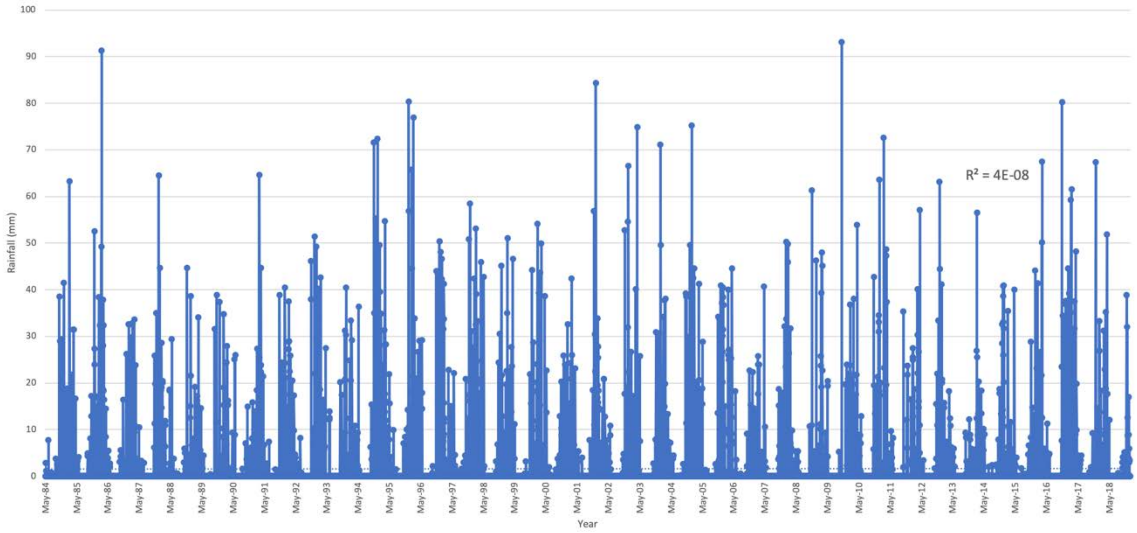

Figure 11: Marsh site daily precipitation values, 1984–2018 (CHIRPS, via GEE).

2. Qualitative Data Results

Qualitative results can be observed in images produced in GEE. For illustration, Fig. 12 shows NDVI for the area surrounding the two study sites, including outline polygons of the two counties, Napa and Solano, that comprise the sites (obtained via the United States Census Bureau TIGER dataset for political boundaries for primary legal divisions for the most recent year, 2016).

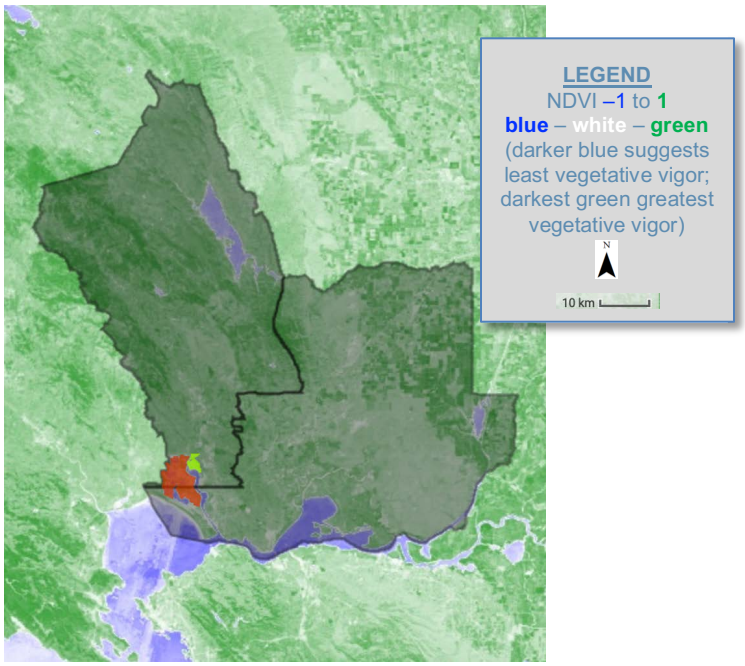

Figure 12: 2018 median NDVI, Napa & Solano counties (grey). Study sights within (red: Marsh; light green: Salt Plant).

The median-pixel NDVI results in the following images are based on the NDVI scale of –1 to 1; the color ramp for the NDVI images runs from blue to white to green, with darkest blue representing –1, or least vegetative vigor (typically water, as it appears in the image), and darkest green representing 1, or greatest vegetative vigor. Arrows point to areas of interest: the violet arrow indicates the Salt Plant site, while the two bottom arrows indicate subareas of the Marsh site.

We can see that from these images that the Salt Plant (violet arrow) has changed modestly to include some vegetation in the intervening years. The black arrow indicates a subsite of the Marsh that shows increased vegetation and the blue arrow indicates a subsite that has become dramatically devegetated. Figs. 13 and 14 allow us to visualize the vegetation/ water distinction at

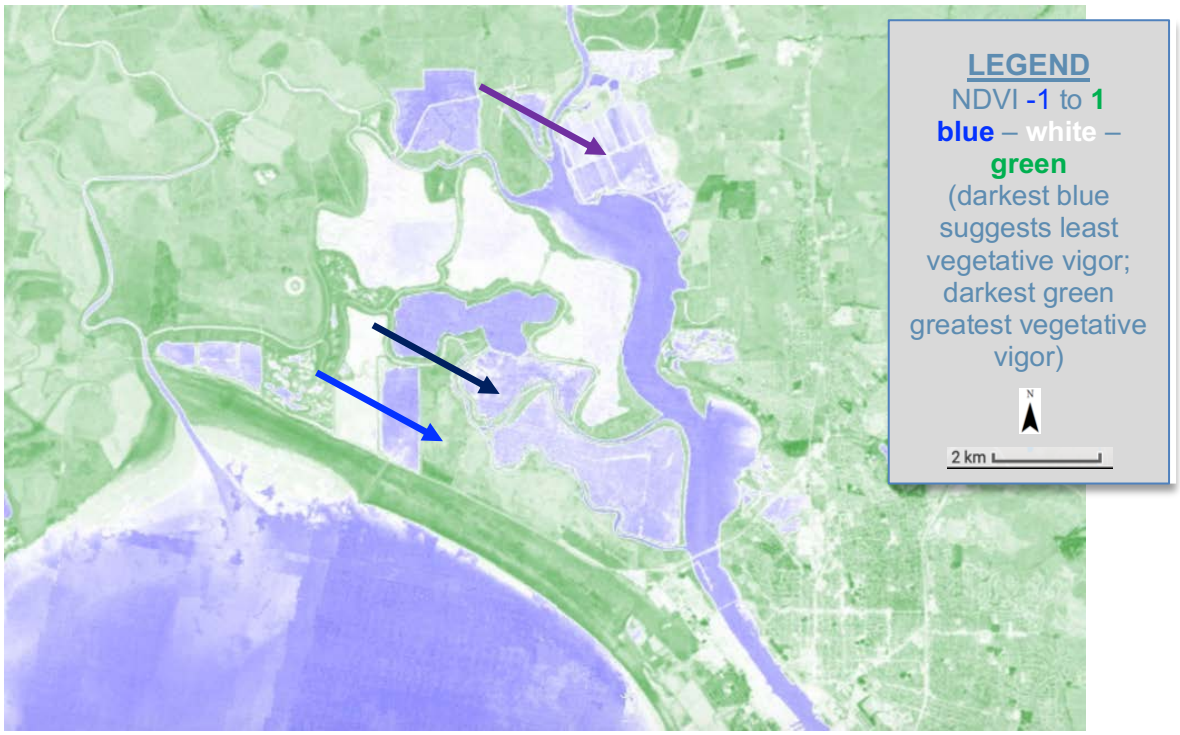

Figure 13: 1984 median NDVI (Landsat 5 TOA).

each stage that is readily apparent. Difference NDVI, however, allows us to see change within a single image; Figs. 15–18 demonstrate difference NDVI for select years. The first two images (Figs. 15 and 16) contrast median annual NDVI values and the second two (Figs. 17 and 18) contrast maximum annual NDVI values.

The maximum NDVI images are the most vivid. Fig. 17 represents the entire study period, and here, the violet arrow shows a complex change in the Salt Plant site – more or less half substantial increase in vegetation, half substantial decrease in vegetation. The Marsh subsite

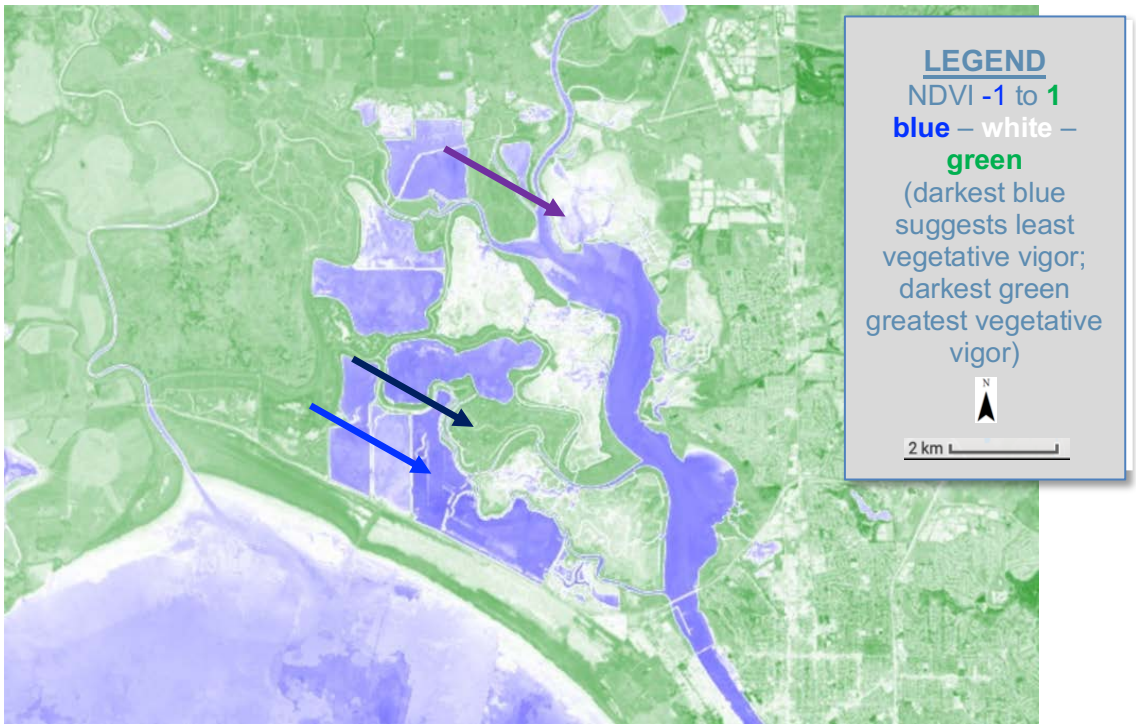

Figure 14: 2018 median NDVI (Landsat 8 TOA).

indicated by the black arrow implies a substantial increase in vegetation, and the Marsh subsite indicated by the blue arrow implies a substantial decrease in vegetation. It is likely that the latter area was purposely flooded by levee breach, though I have been unable to independently verify this as of writing. Most of the change in vegetation for the subsite indicated by the black arrow evidently occurred before 2006, since the change appears substantial in the 1984/ 2018 image, but not the 2006/ 2018 image (Fig. 18, where either stasis or loss of vegetation is indicated). Overall, it is strongly suspected that ponds were designated for the restoration for increased vegetation or new flooding, and that the differences shown here represent those intentions – i.e., are purposeful.

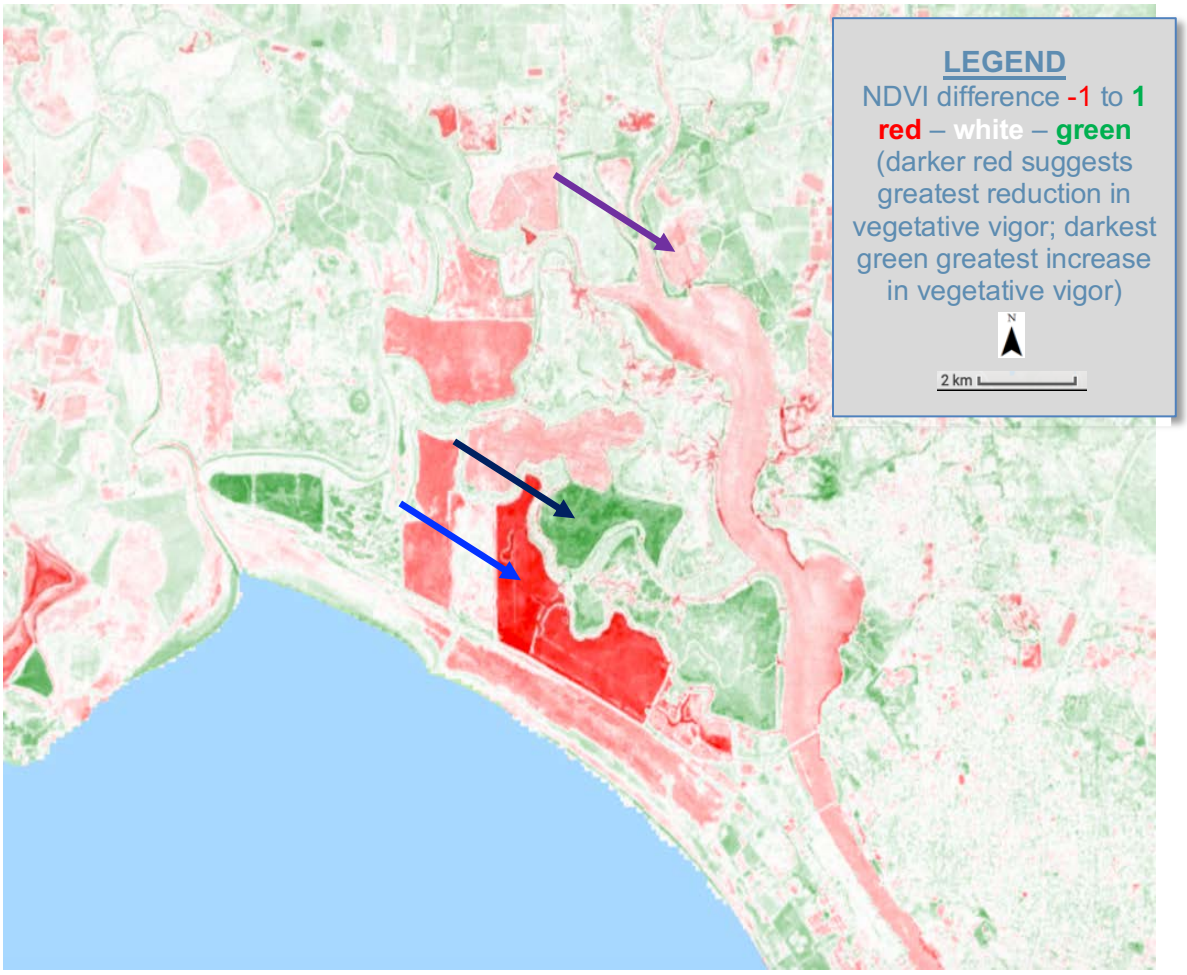

Figure 15: 1984/ 2018 difference median NDVI (Landsats 5, 8 SR).

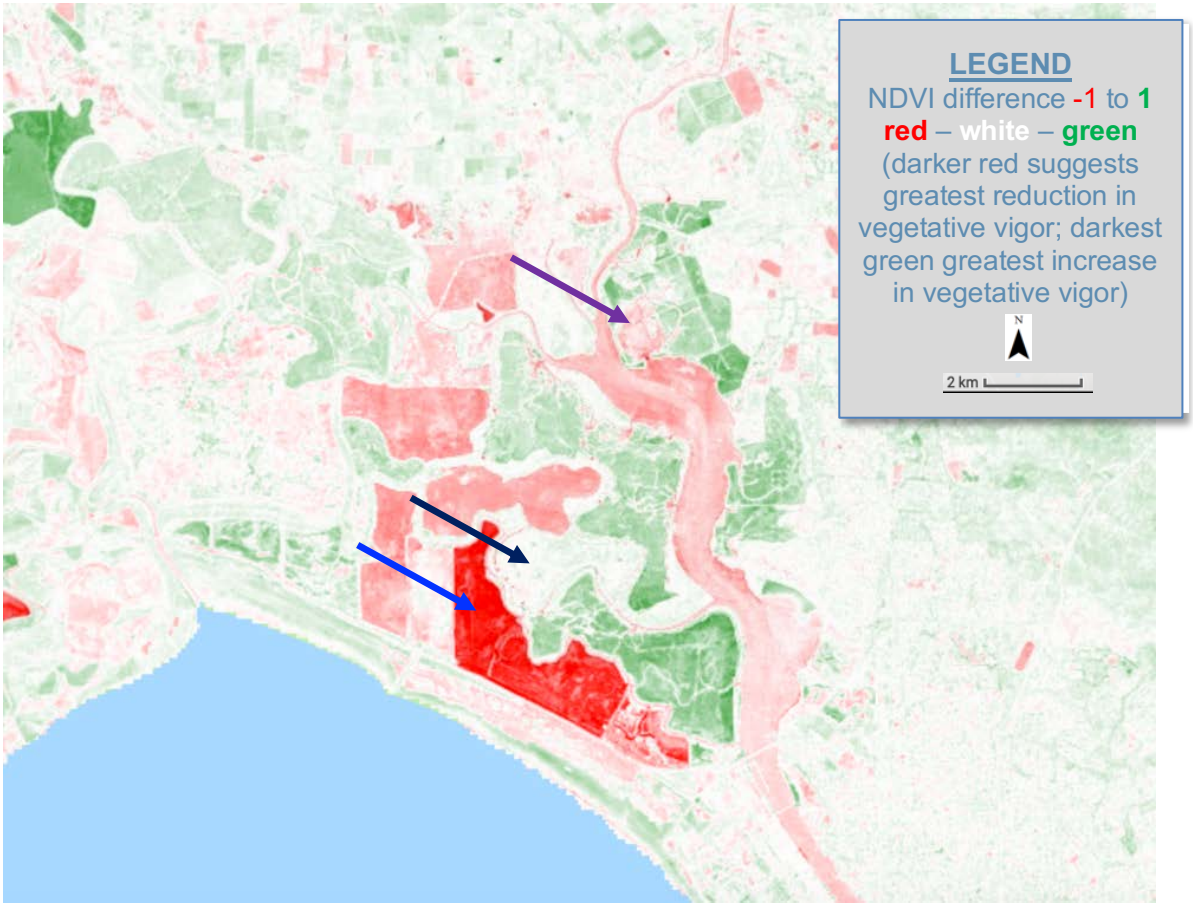

Figure 16: 2006/ 2018 difference median NDVI (Landsats 5, 8 SR).

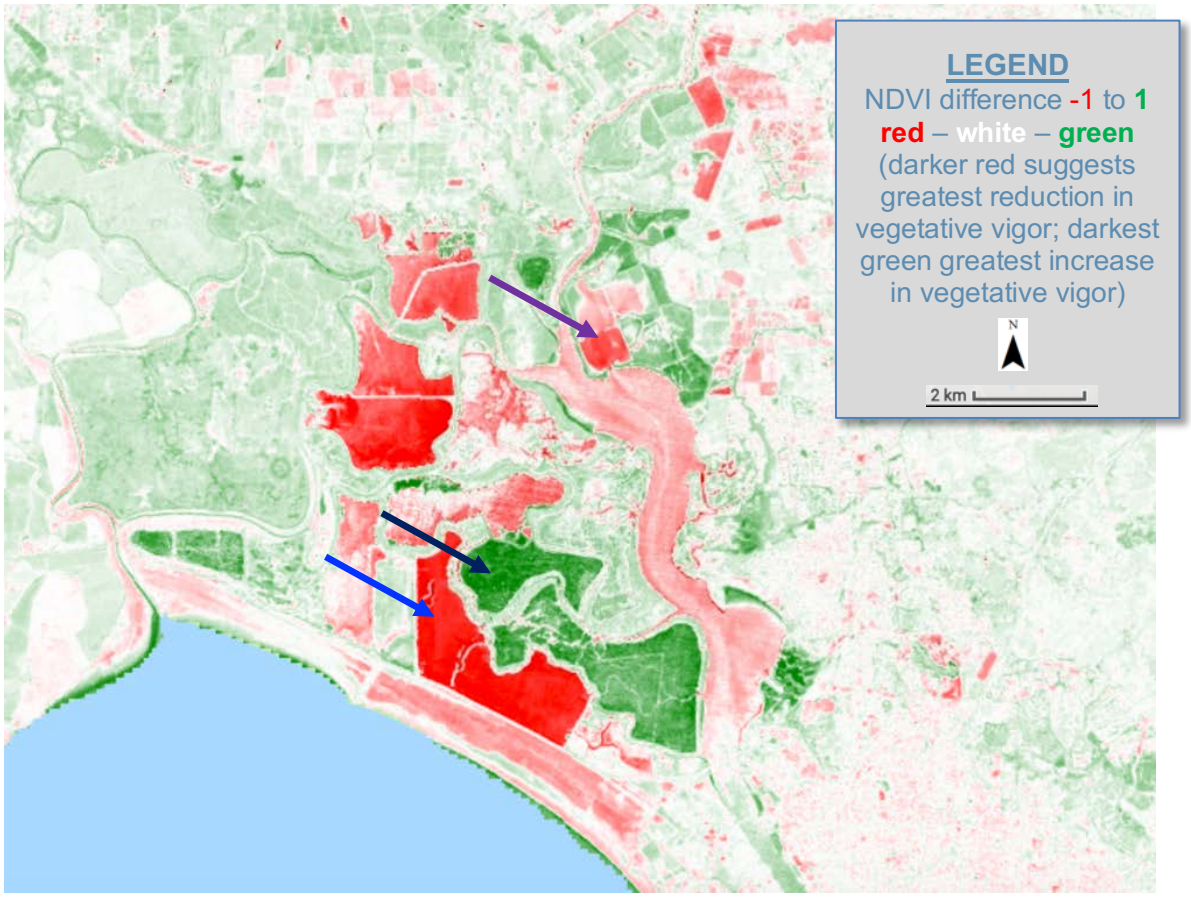

Figure 17: 1984/ 2018 difference max NDVI (Landsats 5, 8 SR).

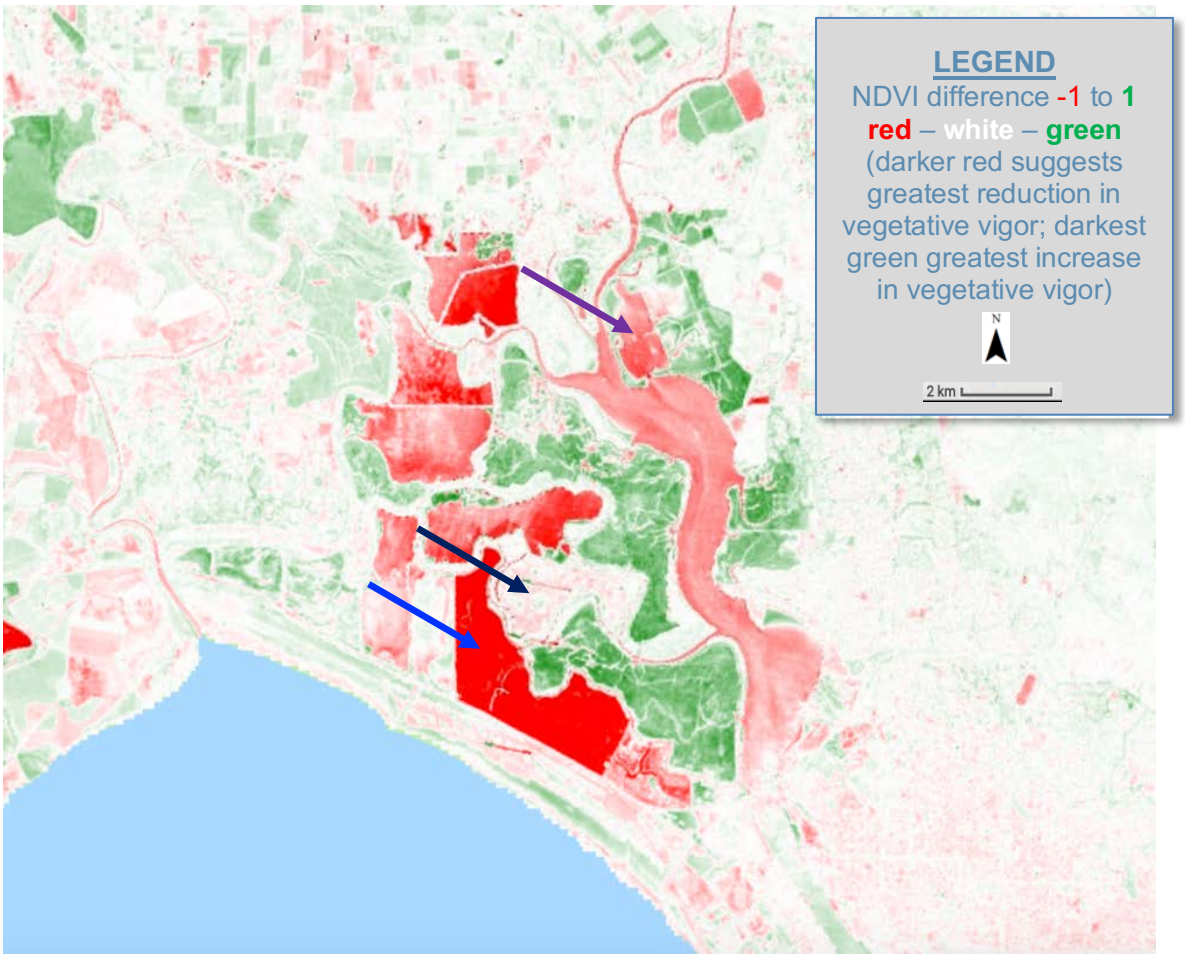

Figure 18: 2006/ 2018 difference max NDVI (Landsats 5, 8 SR).

DISCUSSION

1. Quantitative Results

The quantitative and qualitative results both indicate that the sites, and subsites within each site, are complex and have developed differently. Internal variation presents a challenge not only for restoration, but also for restoration analysis of a large site, especially a site that has notable variation and is early in post-restoration. The qualitative data demonstrates values that vary by pixel, while the quantitative results were averaged across sites. The reductive techniques used here offer great utility for large-scale, automated analysis; but by using values across sites, complexity may be masked.

The data show mixed results for NDVI trends, and this is likely partly due to this complexity, as well as to the lack of post-restoration data due to the restoration's age. Still, for all periods considered, the fact that trends are positive for each site individually (though very weakly so for the last period (2006–18) for the Marsh site) point to an increase in vegetation despite restoration activities like levee breaches. The combined data do not always show positive trends, which is likely an effect of the different site sizes and varying peaks between them.

The fact that the maximum trends are more positive than the median values – though insignificant for the most recent period – is of interest. This indicates that at some point in each later year, the greatest vegetation across the sites was higher than in earlier years. Without further evidence, the more positive results for maximum NDVI imply greater potential as certain plants establish themselves. This is a point that merits further study; it also points to the fact that, for the time being, certain questions may require thorough site sampling to be answered.

A major question that goes unanswered via NDVI analysis is species composition and richness, though these are characteristics that I predict will be remotely analyzable, in a practical way and to some degree, in a generation's time. Such analysis will address whether desired (almost always native) plants have established themselves to the desired degree and whether undesired (invasive) species have entered the site or become more prominent. Post-restoration site monitoring and intervention currently address invasive species for the Napa-Sonoma Marsh; the most recent Biennial Report claims that only small, isolated patches of two invasive species, common reed (*Phragmites australis*) and giant reed grass (*Arundo donax*), have been identified as of 2017, and that they have not spread (Erickson, 2018). Information like this considerably assists remote sensing analysis, because vegetation can be regarded as desirable vegetation. At this point in restoration history, the synergistic relationship of remote and site sampling that is frequently alluded to in the literature is clear.

Rainfall's flat trends, despite periods of drought, implies that the effects are not a result of moisture. This is less surprising given that the Marsh is a tidal wetland, though there are freshwater inputs from the Napa and Sonoma Rivers, and the Salt Plant site is slightly more elevated.

2. Qualitative Results

The intrasite complexity is shown clearly by the differences in the NDVI images and in the automatically computed NDVI difference images; some parts of the Marsh site had reduced vegetation, some increased. The Salt Plant site also demonstrated internal complexity; it often appeared to show more internal gradations, and it is worth repeating that its restoration (2003–10) was later and briefer. For the two sites, these variations may be due to various causes, particularly because the restoration is young, such as the manner in which vegetation spreads

over areas that are no longer delegated to salt production. However, the pattern of vegetation is very likely purposeful, at least in some instances. The Marsh subsites that border each other and are indicated by the blue and black arrows, former salt ponds, demonstrate dramatic divergence. While I have been unable to confirm this, it is highly likely that this divergence was intentional and due to a late flooding, via levee breach, of the subsite indicated by the blue arrow. As indications of intentionality, the demarcated vegetation in the latest images is a reason for optimism. It also demonstrates the power of using NDVI for restoration analysis, even in a site with little vegetation relative to some other sites (e.g., forest).

CONCLUSION

1 Research Question Revisited

By comparing pre- and post-restoration remote sensing data for the Napa-Sonoma Salt Marsh restoration in California, I found that two sites of the larger marsh restoration had mixed results for NDVI values, and that changes depended on subsite and whether median or maximum NDVI was analyzed. Because the restoration is large, is of a type (wetland) that may present singular challenges (e.g., there is less vegetation to analyze), and is early in the post-restoration period, it is unsurprising that the results are mixed. Overall, however, there are two prominent reasons for optimism regarding restoration success in the data: first, there is a significant increasing trend in annual maximum vegetation, with insignificant amounts of this vegetation comprising invasive species; and, second, subareas indicate likely sites of intended vegetation increase or decrease.

This case study, despite being rudimentary in its appraisal, shows that the potential of NDVI for restoration analysis is quite evident, as the qualitative data shows contrasts both stark and subtle. The possibility of automation over long time periods makes the usefulness of NDVI difference studies manifest, and the ability to automatically record maximum NDVI for an entire site for a specified time period is extremely useful. Further, the site could be more finely demarcated if subsite analysis is of interest, and an initial outlay of time in demarcating subsites would offer future time saving. Finally, the ability to automate quantitative data over time periods both long and short is tremendously useful.

Thus, the project research question posed in the Introduction – whether NDVI data obtained via remote sensing are sufficient for restoration success analysis and evaluation – can be answered. Remote sensing data – mainly NDVI, when combined with GIS – is tremendously useful for restoration analysis, particularly when quantitative & qualitative data are utilized together. However, it is rarely sufficient at this time, as restoration analysis also normally requires site sampling for accurate analysis. Even where data is available and a restoration is well established, great internal variation is potentially masked by reductive techniques – which are currently the most feasible approach, particularly for large restorations. These conclusions concur with the pertinent literature, which implies that NDVI offers enormous potential for monitoring wetland restoration but is best supplemented by local observation, with which it synergistic.

Wetlands offer challenges for the use of remote sensing/ GIS techniques such as NDVI, because vegetation is less prominent than in other contexts, such as forests. Given the unique context of wetlands like the one that is the subject of this study, and the fact that the most useful remote sensing and GIS techniques are currently focused on vegetative vigor, the usefulness of remote sensing and GIS for wetlands will lag in comparison to other restoration contexts.

NDVI remains a technique with useful results and one that has high potential for automation. At some point, a more complex web of analysis techniques, such as sophisticated change algorithms, will flourish around it, but it appears to remain the single most useful tool for restoration analysis at this time.

2. Broader Implications for This Restoration

There are clear signs of more demarcated vegetation in the latest images. Because there is reason to believe that it is purposeful, this is reason for optimism, insofar as the effects of a

specific effort are clearly demonstrated in the images. Because the site is a tidal wetland, is a very large project, and is early in the post-restoration period, the sometimes weak (and in on case statistically insignificant) vegetative trends are unsurprising. The caveat is, again, that much internal variation and complexity are probably masked by the reductive techniques here.

However, the fact that annual maximum NDVI showed a more positive trend at least suggests that the site's vegetation is establishing itself. Combined with the site sampling report from 2017 that invasive species are not a substantial problem at this point, the increase in maximum vegetative vigor is assumed to be desirable. There are strongly positive indications for a large tidal salt marsh restoration that has only recently entered post-restoration. Nevertheless, restoration monitoring and analysis will need to occur for several decades before restoration 'success' can be assured.

The restoration faces several major challenges: the ever-increasing human population pressures in the surrounding area, climate change, and the rapid rate of invasive species introductions in San Francisco Bay. Though now over 20 years old, and studying a period that goes back 57 years, a well-known 1998 study is often cited regarding the last challenge (e.g., Cloern & Jassby, 2012); it showed an accelerating rate of invasions in the San Francisco Bay–Delta system, with an introduction every 14 weeks on average (Cohen & Carlton, 1998). Shipping and other vehicles for species communication have only increased since then, so the present rate is likely to be the same or higher. A recent study did indicate that rainy winters appear to reduce invasive species the Bay via a freshwater flush that lowers the salt levels upon which many invasives depend (Chang, Brown, Crooks, & Ruiz, 2018), so the impacts are likely to be complex.

3. Broader Implications for Restoration Analysis Generally

There is strong potential for the use of NDVI, especially for large projects and for projects with a long history – or where, as was the case here, the pre-restoration comparison period was within the period of easily obtainable satellite data. The usefulness of NDVI will depend on the context, however. It is likely most useful, as the literature suggests, in large restorations with ample available data over a long period; further, it is likeliest most useful in high vegetative contexts or in contexts where there are clear expectations for substantial vegetative change.

We will have to wait for other varieties of automated change analysis (e.g., certain algorithms), landscape analysis (elevation, contours), or other VIs, which allow a more complete picture of a restoration. Analysis of species composition and richness are still difficult with remote sensing, and these factors are important elements of restoration 'success'.

A note on available remote sensing data is appropriate. This case study considered only periods since 1984, which was a decision based partly on the fact that satellite photos and specific sensor consistency (via Landsat 5) extends that far, but also partly on the fact that the comparison of interest was pre- and post-restoration; hence, older analysis was deemed less critical. However, it will be desirable for some sites and some projects to have a longer period for comparison. Satellite data, via Landsat, goes back to 1972, though some coverage will be spotty. Consistent airplane photo images reach back earlier in the 20th century.[2] It is conceivable to process air photos, using image software and personal computer GIS software (such as ArcGIS or QGIS),

[2] This study's site is likely much more heavily photographed than the average for a random location on Earth by dint of its proximity to San Francisco. My air photo search, conducted primarily via the University of California Earth Sciences & Map Library and the USDA Aerial Photography Field Office, found relevant air photo sets from the 1940s to 1960s (e.g., Appendix A, Fig. 22).

and upload those images into GEE for analysis alongside satellite photos. It is reasonable to expect that many restoration sites will have data in this fashion, albeit with gaps, to the 1940s. Some sites, particularly urban sites, have complete sets from decades earlier (San Francisco, for example, with air photos from the 1930s or even earlier). Analysis of air photos has a rich history, and recent efforts – see the sampling design methods in Powell et al., 2013 and Powell & Hansen, 2007 for example methods, which offer a rigorous method not unlike site sampling but for an array of remote sensing data – have proven useful for newly analyzing areas remotely.

Further, any remote sensing data obtained in any manner could be processed to align with other data, saved, and added to a GEE database. Qualitative data, via hand-drawn maps and nautical charts, go back centuries, and while I have not observed such attempts, it is not beyond the realm of possibility that some quantitative use could also be made of these images. In this fashion, a slowly growing history of a site could be formed for analysis. The longer the history, the more useful for restoration, particularly given the typical (if unconscious) conviction that 'the older the better' with respect to modeling the 'original' state of a site for restoration.

4. Limitations of the Study

This study has several important limitations. The most important set of limitations result from NDVI's limitations as a tool. First, it depends on assumptions, albeit reasonable ones, about what vegetative vigor signifies and whether NDVI always captures vegetative vigor. Second, variation in species response to NDVI may affect the results, a factor that requires more study. Third, this study's site is a context of relatively low vegetation, which makes decisive analysis more difficult. Relatedly, vegetation increase, though important, is only one blunt piece of evidence. Because species composition and richness is not measured by basic NDVI analysis, for example, undesired (invasive) species may make the results misleading as to restoration 'success'.

Fourth, atmospheric conditions are somewhat surmountable via processing tools, but still may affect data or greatly limit available dates in some contexts. Finally, topographical changes are still difficult to analyze with remote sensing, and my tentative efforts in this study did not achieve useful results in this regard (and so were not included in this paper).

The second set of limitations concerns the extent of data. Further division of the sites into subsites for individual analysis would be enlightening. Reference sites – restorations deemed successful (preferably in the same region), as well as surrounding areas – would provide important comparisons. A workaround for the GEE data aggregation errors encountered for Napa and Solano counties would have made the latter reference possibility surmountable for NDVI comparison. Finally, additional dates for analysis, including via uploaded air photos, would have provided a greater time period for study and pre-restoration reference. The rate of change over additional time span divisions could also have been compared with that data.

5. Future Study

Remote sensing and GIS are advancing markedly. It is likely that within the next generation, technological developments will open many avenues of remote analysis. This includes advances in automated analysis of older historical data (photographs, maps, and charts); computing power, which will allow vaster comparisons (e.g., comparing county-wide NDVI data); algorithms (e.g., change detection like LandTrendr); remote sensing (e.g., more elevation data); and user interfaces (e.g., more user-friendly design for GEE). Such advances will allow easier analysis by remote sensing of evapotranspiration, plant species richness and composition, animal and fungus presence, topography, and hydrology. Finally, automated analysis will make comparison both with surrounding areas and other restorations (benchmark restorations) much more easily accessible.

This study offers a very small link in a chain of evidence that supports the prospect of utilizing remote sensing and GIS for restoration analysis. However, each of these elements above requires both development and future study. With respect to the Napa-Sonoma Marsh, another ten to twenty years will better reveal the strength of the restoration, particularly in the face of the challenges mentioned above. For now, site sampling remains a critical component of analysis.

6. Final Reflection

We should occasionally return to questions about the philosophical underpinnings of the activity under study. What is good for the Marsh, and what is 'restoration'? If the Marsh does succumb to non-native species, for instance, but serves the once-lost functions of a (healthy) tidal salt marsh – particularly in the context of a great bay system that has been heavily modified by human presence – does that achieve 'restoration'? What are the limits of 'success' for a restoration? If new evidence of a longer-ago past for the site is found that is substantially different from the goals established for the restoration in 1994, should the restoration be artificially modified again?

Neither NDVI nor any other remote sensing technique, whether they become more adept at reflecting the state and change of restoration or do not, can address these sorts of questions. Restoration analysis and evaluation will always include social, normative elements.

REFERENCES CITED

Abtew, W., & Melesse, A. (2013). Wetland restoration assessment using remote sensing- and surface energy budget-based evapotranspiration. In W. Abtew & A. Melesse (Eds.), *Evaporation and Evapotranspiration: Measurements and Estimations* (pp. 177–195). https://doi.org/10.1007/978-94-007-4737-1_12

Ballanti, L., Byrd, K. B., Woo, I., & Ellings, C. (2017). Remote sensing for wetland mapping and historical change detection at the Nisqually River Delta. *Sustainability*, *9*(11), 1919.

Barnum, A. (1996, October 25). Bay Area's Wetland Renaissance: Government, business, conservationists collaborate. *San Francisco Chronicle*, p. A1.

Batzer, D. P., & Sharitz, R. R. (2014). *Ecology of freshwater and estuarine wetlands* (2nd edition; ebook). Univ of California Press.

Campbell, J. B., & Wynne, R. H. (2011). *Introduction to Remote Sensing*. Guilford Press.

Carroll, D. (2007). Napa-Sonoma Marshes. *Bay Nature*, *7*(3), 36–36.

Chang, A. L., Brown, C. W., Crooks, J. A., & Ruiz, G. M. (2018). Dry and wet periods drive rapid shifts in community assembly in an estuarine ecosystem. *Global Change Biology*, *24*(2), e627–e642. https://doi.org/10.1111/gcb.13972

Cloern, J. E., & Jassby, A. D. (2012). Drivers of change in estuarine-coastal ecosystems: Discoveries from four decades of study in San Francisco Bay. *Reviews of Geophysics*, *50*(4).

Cohen, A. N., & Carlton, J. T. (1998). Accelerating Invasion Rate in a Highly Invaded Estuary. *Science*, *279*(5350), 555–558. https://doi.org/10.1126/science.279.5350.555

Erickson, G. (2018). *2017 Biennial Report for the Napa River Salt Marsh Restoration Project and Napa River Plant Site Restoration Project, Napa-Sonoma Marshes Wildlife Area*. Retrieved from

California State Coastal Conservancy website: http://scc.ca.gov/napa-river-salt-marsh-restoration-project-progress-to-date/

Google. (n.d.). Google Earth Engine API. Retrieved April 27, 2019, from Google Developers website: https://developers.google.com/earth-engine/

Hu, S., Niu, Z., Chen, Y., Li, L., & Zhang, H. (2017). Global wetlands: Potential distribution, wetland loss, and status. *Science of The Total Environment*, *586*, 319–327. https://doi.org/10.1016/j.scitotenv.2017.02.001

Huffman, T. (1999). The Napa-Sonoma Marshes: Then and Now. *Outdoor California*, 9–12.

Josselyn, M. (1983). *The Ecology of San Francisco Bay Tidal Marshes: A Community Profile* (No. FWS-/OBHS-83/23). Tiburon Center for Environmental Studies, San Francisco State University; U.S. Fish and Wildlife Service.

Klemas, V. (2011). Remote sensing of wetlands: Case studies comparing practical techniques. *Journal of Coastal Research*, *27*(3), 418–427.

Klemas, V. (2013). Using remote sensing to select and monitor wetland restoration sites: An overview. *Journal of Coastal Research*, *29*(4), 958–970.

Knox, S. H., Dronova, I., Sturtevant, C., Oikawa, P. Y., Matthes, J. H., Verfaillie, J., & Baldocchi, D. (2017). Using digital camera and Landsat imagery with eddy covariance data to model gross primary production in restored wetlands. *Agricultural and Forest Meteorology*, *237*, 233–245.

Landers, J. (2003). Salt pond restoration to benefit San Francisco Bay. *Civil Engineering*, *73*(2), 26.

Lumbierres, M., Méndez, P. F., Bustamante, J., Soriguer, R., & Santamaría, L. (2017). Modeling Biomass Production in Seasonal Wetlands Using MODIS NDVI Land Surface Phenology. *Remote Sensing*, *9*(4), 392. https://doi.org/10.3390/rs9040392

Measuring Vegetation (NDVI & EVI). (2000, August 30). Retrieved April 6, 2019, from https://earthobservatory.nasa.gov/features/MeasuringVegetation/measuring_vegetation_4.php

NASA. (2019, April 24). Landsat 7. Retrieved April 24, 2019, from Landsat Science: Landsat 7 website: https://landsat.gsfc.nasa.gov/landsat-7/

Newcomer, M. E., Kuss, A. J. M., Ketron, T., Remar, A., Choksi, V., & Skiles, J. W. (2014). Estuarine sediment deposition during wetland restoration: A GIS and remote sensing modeling approach. *Geocarto International*, *29*(4), 451–467.

Phinn, S. R., Stow, D. A., & Zedler, J. B. (1996). Monitoring wetland habitat restoration in southern California using airborne multi spectral video data. *Restoration Ecology*, *4*(4), 412–422.

Powell, S. L., & Hansen, A. J. (2007). Conifer Cover Increase in the Greater Yellowstone Ecosystem: Frequency, Rates, and Spatial Variation. *Ecosystems*, *10*(2), 204–216. Retrieved from JSTOR.

Powell, S. L., Hansen, A. J., Rodhouse, T. J., Garrett, L. K., Betancourt, J. L., Dicus, G. H., & Lonneker, M. K. (2013). Woodland Dynamics at the Northern Range Periphery: A Challenge for Protected Area Management in a Changing World. *PLOS ONE*, *8*(7), e70454. https://doi.org/10.1371/journal.pone.0070454

Riegel, J. B., Bernhardt, E., & Swenson, J. (2013). Estimating above-ground carbon biomass in a newly restored coastal plain wetland using remote sensing. *PloS One*, *8*(6), e68251.

San Francisco Bay Joint Venture. (2018). Napa Sonoma-Marshes Wildlife Area Napa Plant Site Restoration Project. Retrieved October 24, 2018, from http://www.sfbayjv.org/project-napa-sonoma-marshes.php

Saving the Bay: The story of San Francisco Bay. (2009). San Francisco: Ronald M. Blatman, Inc., and KQED/KTEH public television.

Selvam, V., Ravichandran, K. K., Gnanappazham, L., & Navamuniyammal, M. (2003). Assessment of community-based restoration of Pichavaram mangrove wetland using remote sensing data. *Current Science*, *85*(6), 794–798.

Shuman, C. S., & Ambrose, R. F. (2003). A comparison of remote sensing and ground-based methods for monitoring wetland restoration success. *Restoration Ecology*, *11*(3), 325–333.

Sloan, D. (2006). *Geology of the San Francisco Bay Region*. Univ of California Press.

StackOverflow: Google Earth Engine. (n.d.). Retrieved April 28, 2019, from Stack Overflow website: https://stackoverflow.com/questions/tagged/google-earth-engine

Tuxen, K. A., Schile, L. M., Kelly, M., & Siegel, S. W. (2008). Vegetation colonization in a restoring tidal marsh: A remote sensing approach. *Restoration Ecology*, *16*(2), 313–323.

APPENDICES

APPENDIX A

ADDITIONAL IMAGES

Figure 19: 1850 Chart of the Bay of San Pablo Straits of Carquines and part of the Bay of San Francisco California*, US Navy nautical chart (National Oceanic and Atmospheric Administration, n.d.).*

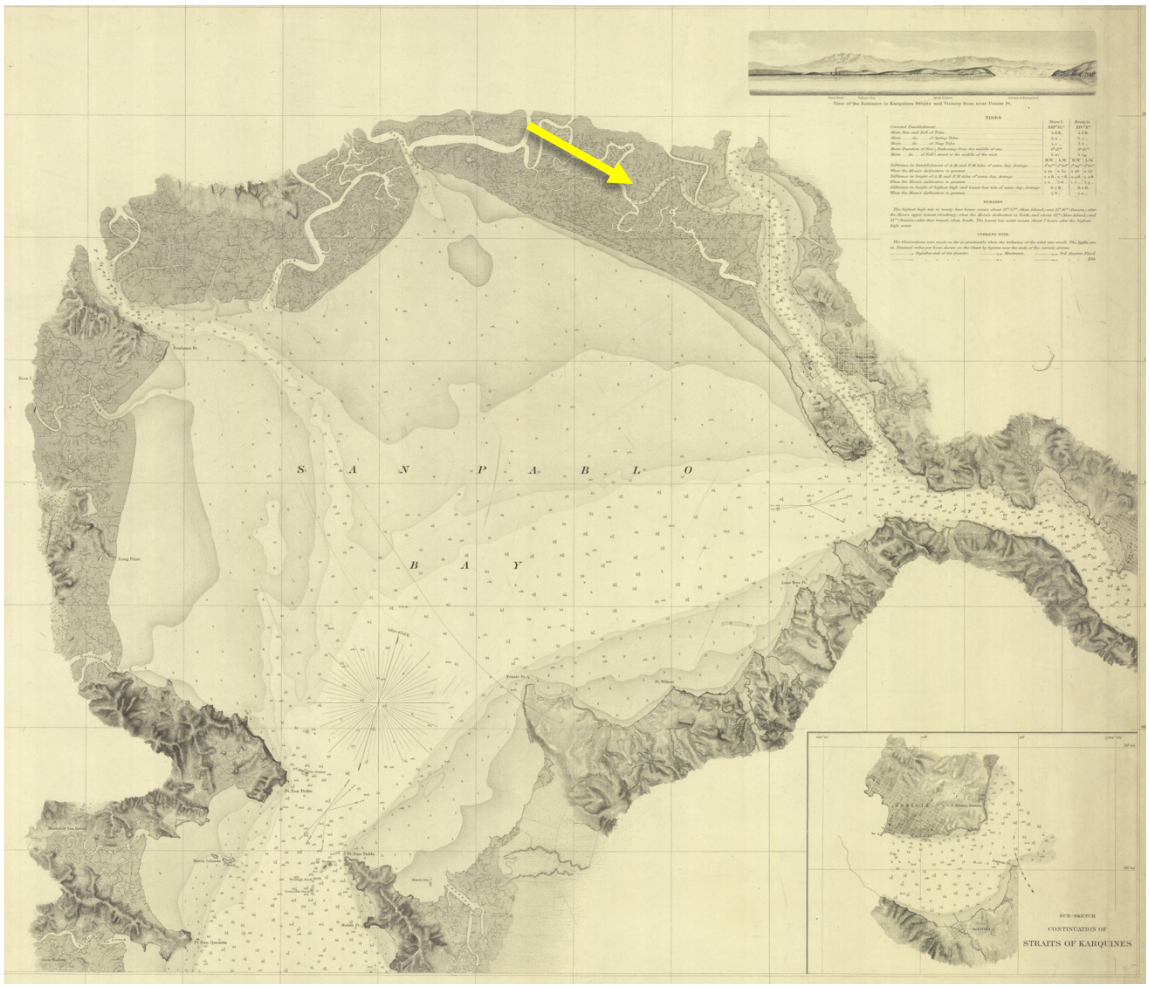

Figure 20: 1863 San Pablo Bay Nautical Chart (National Oceanic and Atmospheric Administration, n.d.).

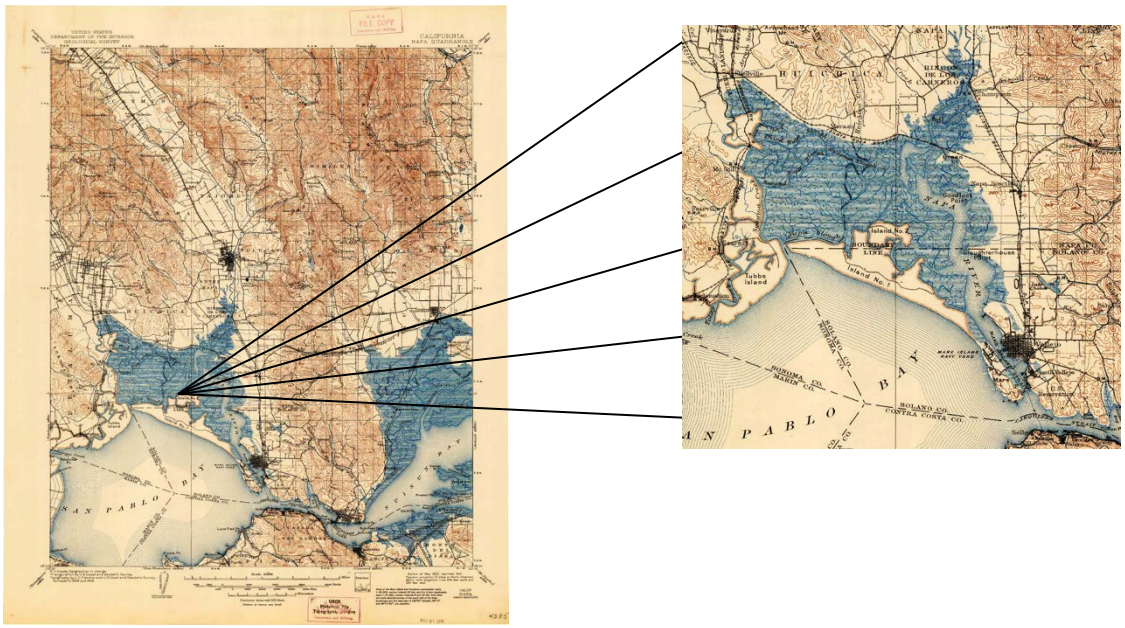

Figure 21: 1902, Napa Quadrangle *(United States Geological Survey, n.d.).*

Figure 22: 1965 air photos of site. 'Sonoma, Solano, Marin, Napa, Contra Costa', Bay Area Transportation Study Commission, May 1965. Courtesy of the University of California Earth Sciences & Map Library.

APPENDIX B

GOOGLE EARTH ENGINE CODE

Two site polygons constructed in GEE (Fig. 6)

```
var marsh: Polygon, 220 vertices
var salt_plant: Polygon, 54 vertices

// The correspond to:
var marsh = /* color: #d63000 */ee.Geometry.Polygon(
        [[[-122.36441215959906, 38.142213705332395],
        // … further vertex coordinates omitted for brevity.

salt_plant = /* color: #98ff00 */ee.Geometry.Polygon(
        [[[-122.30758752235027, 38.184218791093826],
        // … further vertex coordinates omitted for brevity.
```

Combined sites, NDVI charts (Landsats 5, 7, & 8 SR) (Figs. 7–10)

Data was downloaded using three scripts in GEE, for Landsats 5, 7, & 8. The first, for Landsat 5, is listed here (the other two use corresponding Landsat designations, but are otherwise identical).

```
var marsh: Polygon, 220 vertices
var salt_plant: Polygon, 54 vertices
var l5sr: ImageCollection "USGS Landsat 5 Surface Reflectance Tier 1"

// Center on the Napa-Sonoma Marsh.
Map.setCenter(-122.320981, 38.161243, 11);

// This field contains UNIX time in milliseconds.
var timeField = 'system:time_start';

// Use this function to add variables for NDVI, time and a constant to
Landsat 5 imagery.
var addVariables = function(image) {
   // Compute time in fractional years since the epoch.
   var date = ee.Date(image.get(timeField));
   var years = date.difference(ee.Date('1970-01-01'), 'year');
   // Return the image with the added bands.
   return image
      // Add an NDVI band.
      .addBands(image.normalizedDifference(['B4', 'B3']).rename('NDVI'))
.float()
      // Add a time band.
      .addBands(ee.Image(years).rename('t').float())
      // Add a constant band.
      .addBands(ee.Image.constant(1));
};

// Add variables and filter to the area of interest.
var filteredLandsat = l5sr
   .filterBounds(marsh)
   .map(addVariables);

// Plot a time series of NDVI at a single location.
var l5Chart_marsh = ui.Chart.image.series(filteredLandsat.select('NDVI'),
marsh)
```

```
   .setChartType('ScatterChart')
   .setOptions({
      title: 'USGS Landsat 5 Surface Reflectance Tier 1 NDVI time series at
Marsh',
      trendlines: {0: {
         color: 'CC0000'
      }},
      lineWidth: 1,
      pointSize: 3,
   });
print(l5Chart_marsh);

// Add variables and filter to the area of interest.
var filteredLandsat = l5sr
   .filterBounds(salt_plant)
   .map(addVariables);

// Plot a time series of NDVI at a single location.
var l5Chart_salt_plant =
ui.Chart.image.series(filteredLandsat.select('NDVI'), salt_plant)
   .setChartType('ScatterChart')
   .setOptions({
      title: 'USGS Landsat 5 Surface Reflectance Tier 1 NDVI time series at
Salt Plant',
      trendlines: {0: {
         color: 'CC0000'
      }},
      lineWidth: 1,
      pointSize: 3,
   });
print(l5Chart_salt_plant);
```

Marsh site daily precipitation values, 1984–2018 (CHIRPS) (Fig. 11)

Due to the size of the data aggregation, data was downloaded piecemeal using three scripts for the CHIRPS dataset: 1995–2004, 2005–14, and 2015–18. The first is listed here (the other two are identical save for dates). The data was merged and analyzed in Microsoft Excel.

```
var marsh: Polygon, 220 vertices
var salt_plant: Polygon, 54 vertices
var chirps: ImageCollection "CHIRPS Daily: Climate Hazards Group InfraRed
Precipitation with Station Data (version 2.0 final)"

// Get Climate Hazards Group InfraRed Precipitation with Station data
(CHIRPS).
var dataset = ee.ImageCollection(chirps)
                  .filter(ee.Filter.date('1994-12-31', '2004-12-31'));
var precipitation = dataset.select('precipitation');

// Plot a time series of rainfall for Marsh.
var rainfall_marsh = ui.Chart.image.series(precipitation, marsh)
   .setChartType('ScatterChart')
```

```
   .setOptions({
      title: 'Rainfall time series at Marsh',
      trendlines: {0: {
         color: 'CC0000'
      }},
      lineWidth: 1,
      pointSize: 3,
   });
print(rainfall_marsh);
```

2018 median NDVI, Napa & Solano counties (grey). Study sights within (red: Marsh; light green: Salt Plant) (Fig. 12)

As noted in the text, the NDVI time series was incomputable in GEE, as the data was too extensive to aggregate. Hence, the time series language, which was originally present, has been removed from this script.

```
var marsh: Polygon, 220 vertices
var salt_plant: Polygon, 54 vertices
var l8toa: ImageCollection "USGS Landsat 8 Collection 1 Tier 1 TOA
Reflectance" (12 bands)

// Zoom & center.
Map.setCenter(-122.320981, 38.161243, 9);

// Get the median over time, in each band, in each pixel.
var median = l8toa.filterDate('2018-01-01', '2018-12-31').median();

// Make a variable of visualization parameters.
var visParams = {bands: ['B4', 'B3', 'B2'], max: 0.3};

// Display the median composite.
Map.addLayer(median, visParams, 'median');

// Calculate NDVI.
var ndvi = median.normalizedDifference(['B5', 'B4']);

// Display the result using a color ramp of blue-white-green.
var ndviParams = {min: -1, max: 1, palette: ['blue', 'white', 'green']};
Map.addLayer(ndvi, ndviParams, 'NDVI');

// Load the counties: Napa and Sonoma polygons.
var napa = ee.FeatureCollection('TIGER/2016/Counties')
  .filter(ee.Filter.eq('NAME', 'Napa'));
print(napa);
var table = napa;
Map.addLayer(table);
var solano = ee.FeatureCollection('TIGER/2016/Counties')
  .filter(ee.Filter.eq('NAME', 'Solano'));
print(napa);
var table2 = solano;
Map.addLayer(table2);
```

1984 median NDVI (Landsat 5 TOA) (Fig. 13)

```
var marsh: Polygon, 220 vertices
var salt_plant: Polygon, 54 vertices
var l5toa: ImageCollection "USGS Landsat 5 TM Collection 1 Tier 1 TOA
Reflectance" (8 bands)

// Center on the Napa-Sonoma Marsh.
Map.setCenter(-122.320981, 38.161243, 11);

// Get the median over time, in each band, in each pixel.
var median = l5toa.filterDate('1984-01-01', '1984-12-31').median();

// Make a variable of visualization parameters.
var visParams = {bands: ['B3', 'B2', 'B1'], max: 0.3};

// Display the median composite.
Map.addLayer(median, visParams, 'median');

// Calculate NDVI.
var ndvi = median.normalizedDifference(['B4', 'B3']);

// Display the result using a color ramp of blue-white-green.
var ndviParams = {min: -1, max: 1, palette: ['blue', 'white', 'green']};
Map.addLayer(ndvi, ndviParams, 'NDVI for median');
```

2018 median NDVI (Landsat 8 TOA) (Fig. 14)

```
var marsh: Polygon, 220 vertices
var salt_plant: Polygon, 54 vertices
var l8toa: ImageCollection "USGS Landsat 8 Collection 1 Tier 1 TOA
Reflectance" (12 bands)

// Center map on sites with appropriate zoom.
Map.setCenter(-122.320981, 38.161243, 11);

// Get the median over time, in each band, in each pixel.
var median = l8toa.filterDate('2018-01-01', '2018-12-31').median();

// Make a variable of visualization parameters.
var visParams = {bands: ['B4', 'B3', 'B2'], max: 0.3};

// Display the median composite as a map layer.
Map.addLayer(median, visParams, 'median');

// Calculate NDVI.
var ndvi = median.normalizedDifference(['B5', 'B4']);

// Display the result using a color ramp of blue-white-green.
var ndviParams = {min: -1, max: 1, palette: ['blue', 'white', 'green']};
Map.addLayer(ndvi, ndviParams, 'NDVI for median');
```

1984/ 2018 difference median NDVI (Landsats 5, 8 SR) (Fig. 15)

```
var marsh: Polygon, 220 vertices
var salt_plant: Polygon, 54 vertices
var l5sr: ImageCollection "USGS Landsat 5 Surface Reflectance Tier 1"
var l8sr: ImageCollection "USGS Landsat 8 Surface Reflectance Tier 1"

// Get the median over time, in each band, in each pixel, 1984.
var median_1984 = ee.Image(
  l5sr.filterBounds(marsh)
    .filterDate('1984-01-01', '1984-12-31')
    .median()
);

// Get the median over time, in each band, in each pixel, 2018.
var median_2018 = ee.Image(
  l8sr.filterBounds(marsh)
    .filterDate('2018-01-01', '2018-12-31')
    .median()
);

// Get NDVI from Landsat 5 imagery for 1st year.
var getNDVI_1984 = function(median_1984) {
  return median_1984.normalizedDifference(['B4', 'B3']);
};

// Get NDVI from Landsat 8 imagery for 2nd year.
var getNDVI_2018 = function(median_2018) {
  return median_2018.normalizedDifference(['B5', 'B4']);
};

// Compute NDVI from the scenes.
var ndvi1 = getNDVI_1984(median_1984);
var ndvi2 = getNDVI_2018(median_2018);

// Compute the difference in NDVI.
var ndviDifference = ndvi2.subtract(ndvi1);
// Load the land mask from the SRTM DEM.
var landMask = ee.Image('CGIAR/SRTM90_V4').mask();

// Update the NDVI difference mask with the land mask.
var maskedDifference = ndviDifference.updateMask(landMask);

// Display the masked result.
var vizParams = {min: -1, max: 1, palette: ['red', 'white', 'green']};
Map.setCenter(-122.320981, 38.161243, 12);
Map.addLayer(maskedDifference, vizParams, 'NDVI difference, median');
```

2006/ 2018 difference median NDVI (Landsats 5, 8 SR) (Fig. 16)

```
var marsh: Polygon, 220 vertices
var salt_plant: Polygon, 54 vertices
var l5sr: ImageCollection "USGS Landsat 5 Surface Reflectance Tier 1"
var l8sr: ImageCollection "USGS Landsat 8 Surface Reflectance Tier 1"

// Get the median over time, in each band, in each pixel, 2006.
var median_2006 = ee.Image(
```

```
  l5sr.filterBounds(marsh)
    .filterDate('2006-01-01', '2006-12-31')
    .median()
);

// Get the median over time, in each band, in each pixel, 2018.
var median_2018 = ee.Image(
  l8sr.filterBounds(marsh)
    .filterDate('2018-01-01', '2018-12-31')
    .median()
);

// Get NDVI from Landsat 5 imagery for 1st year.
var getNDVI_2006 = function(median_2006) {
  return median_2006.normalizedDifference(['B4', 'B3']);
};

// Get NDVI from Landsat 8 imagery for 2nd year.
var getNDVI_2018 = function(median_2018) {
  return median_2018.normalizedDifference(['B5', 'B4']);
};

// Compute NDVI from the scenes.
var ndvi1 = getNDVI_2006(median_2006);
var ndvi2 = getNDVI_2018(median_2018);

// Compute the difference in NDVI.
var ndviDifference = ndvi2.subtract(ndvi1);
// Load the land mask from the SRTM DEM.
var landMask = ee.Image('CGIAR/SRTM90_V4').mask();

// Update the NDVI difference mask with the land mask.
var maskedDifference = ndviDifference.updateMask(landMask);

// Display the masked result.
var vizParams = {min: -1, max: 1, palette: ['red', 'white', 'green']};
Map.setCenter(-122.320981, 38.161243, 12);
Map.addLayer(maskedDifference, vizParams, 'NDVI difference, median');
```

1984/ 2018 difference max NDVI (Landsats 5, 8 SR) (Fig. 17)

```
var marsh: Polygon, 220 vertices
var salt_plant: Polygon, 54 vertices
var l5sr: ImageCollection "USGS Landsat 5 Surface Reflectance Tier 1"
var l8sr: ImageCollection "USGS Landsat 8 Surface Reflectance Tier 1"

// Get the max NDVI [determined via previously downloaded data] for 1984:
date is 1984-10-25.
var max_1984 = ee.Image(
  l5sr.filterBounds(marsh)
    .filterDate('1984-10-25', '1984-10-26')
    .median()
);

// Get the max NDVI [determined via previously downloaded data] for 2018:
date is 2018-08-04.
```

```
var max_2018 = ee.Image(
  l8sr.filterBounds(marsh)
    .filterDate('2018-08-04', '2018-08-05')
    .median()
);

// Get NDVI from Landsat 5 imagery for the 1st date.
var getNDVI_1984 = function(max_1984) {
  return max_1984.normalizedDifference(['B4', 'B3']);
};

// Get NDVI from Landsat 8 imagery for 2nd year.
var getNDVI_2018 = function(max_2018) {
  return max_2018.normalizedDifference(['B5', 'B4']);
};

// Compute NDVI from the scenes.
var ndvi1 = getNDVI_1984(max_1984);
var ndvi2 = getNDVI_2018(max_2018);

// Compute the difference in NDVI.
var ndviDifference = ndvi2.subtract(ndvi1);
// Load the land mask from the SRTM DEM.
var landMask = ee.Image('CGIAR/SRTM90_V4').mask();

// Update the NDVI difference mask with the land mask.
var maskedDifference = ndviDifference.updateMask(landMask);

// Display the masked result.
var vizParams = {min: -1, max: 1, palette: ['red', 'white', 'green']};
Map.setCenter(-122.320981, 38.161243, 2);
Map.addLayer(maskedDifference, vizParams, 'NDVI difference, max');
```

2006/ 2018 difference max NDVI (Landsats 5, 8 SR) (Fig. 18)

```
var marsh: Polygon, 220 vertices
var salt_plant: Polygon, 54 vertices
var l5sr: ImageCollection "USGS Landsat 5 Surface Reflectance Tier 1"
var l8sr: ImageCollection "USGS Landsat 8 Surface Reflectance Tier 1"

// Get the max NDVI [determined via previously downloaded data] for 2006:
date is 2006-07-25 (but range used here because images turn out to be
incomplete for 2006-07-25).
var max_2006 = ee.Image(
  l5sr.filterBounds(marsh)
    .filterDate('2006-07-18', '2006-07-26')
    .median()
);

// Get the max NDVI [determined via previously downloaded data] for 2018:
date is 2018-08-04.
var max_2018 = ee.Image(
  l8sr.filterBounds(marsh)
    .filterDate('2018-08-04', '2018-08-05')
    .median()
);
```

```
// Get NDVI from Landsat 5 imagery for the 1st date.
var getNDVI_2006 = function(max_2006) {
  return max_2006.normalizedDifference(['B4', 'B3']);
};

// Get NDVI from Landsat 5 imagery for 2nd year.
var getNDVI_2018 = function(max_2018) {
  return max_2018.normalizedDifference(['B5', 'B4']);
};

// Compute NDVI from the scenes.
var ndvi1 = getNDVI_2006(max_2006);
var ndvi2 = getNDVI_2018(max_2018);

// Compute the difference in NDVI.
var ndviDifference = ndvi2.subtract(ndvi1);
// Load the land mask from the SRTM DEM.
var landMask = ee.Image('CGIAR/SRTM90_V4').mask();

// Update the NDVI difference mask with the land mask.
var maskedDifference = ndviDifference.updateMask(landMask);

// Display the masked result.
var vizParams = {min: -1, max: 1, palette: ['red', 'white', 'green']};
Map.setCenter(-122.320981, 38.161243, 12);
Map.addLayer(maskedDifference, vizParams, 'NDVI difference, max');
```